AGU PUBLICATIONS

Water Resources Research

RESEARCH ARTICLE

10.1002/2013WR014400

Key Points:
- We modeled streams with restored floodplains (FP) and hyporheic zones (HZ)
- FP had more exchange but HZ had longer residence times more of the year
- FP and HZ are different but neither may benefit dissolved pollutant removal

Supporting Information:
- Readme
- Table S1
- Table S2
- Table S3
- Table S4
- Table S5

Correspondence to:
E. T. Hester,
ehester@vt.edu

Citation:
Azinheira, D. L., D. T. Scott, W. Hession, and E. T. Hester (2014), Comparison of effects of inset floodplains and hyporheic exchange induced by in-stream structures on solute retention, *Water Resour. Res.*, *50*, doi:10.1002/2013WR014400.

Received 17 JUL 2013
Accepted 2 JUL 2014
Accepted article online 7 JUL 2014

Comparison of effects of inset floodplains and hyporheic exchange induced by in-stream structures on solute retention

David L. Azinheira[1], Durelle T. Scott[2], W. Hession[2], and Erich T. Hester[1]

[1]Department of Civil and Environmental Engineering, Virginia Tech, Blacksburg, Virginia, USA, [2]Department of Biological Systems Engineering, Virginia Tech, Blacksburg, Virginia, USA

Abstract The pollution of streams and rivers is a growing concern, and environmental guidance increasingly suggests stream restoration to improve water quality. Solute retention in off-channel storage zones, such as hyporheic zones and floodplains, is typically necessary for significant reaction to occur. Yet, the effects of two common restoration techniques, in-stream structures and inset floodplains, on solute retention have not been rigorously compared. We used MIKE SHE to model hydraulics and solute transport in the channel, on inset floodplains, and in structure-induced hyporheic zones of a third-order stream. We varied hydraulic conditions (winter base flow, summer base flow, and stormflow), geology (hydraulic conductivity), and stream restoration design parameters (inset floodplain length and presence of in-stream structures). The in-stream structures induced hyporheic exchange for approximately 20% of the year (during summer base flow) while inset floodplains were active for approximately 1% of the year (during stormflow). Flow onto inset floodplains and residence times in both the channel and on the floodplains increased nonlinearly with the fraction of bank with floodplains installed. The fraction of streamflow that flowed onto the inset floodplains was 1–3 orders of magnitude higher than that which flowed through the structure-induced hyporheic zone. Yet, residence times and mass storage in the hyporheic zone were 1–5 orders of magnitude larger than that on individual inset floodplains. In our modeling, neither in-stream structures nor inset floodplains had sufficient percent flow and residence times *simultaneously* to have a substantial impact on dissolved contaminants flowing downstream.

1. Introduction

1.1. Stream Restoration Goals and Techniques

The degradation of streams and rivers in the U.S. is well documented [*FISRWG*, 1998], and stream restoration is a flourishing industry [*Bernhardt et al.*, 2005]. Typical objectives of restoration include improving bank stability [*Buchanan et al.*, 2012], aesthetics [*Kondolf and Micheli*, 1995], habitat creation [*Box*, 1996; *Roni et al.*, 2002], and water quality [*Craig et al.*, 2008; *Filoso and Palmer*, 2011]. Stream restoration projects are often implemented to mitigate impacts elsewhere [*BenDor et al.*, 2009], to create habitat under the Endangered Species Act [*Roni et al.*, 2002], and increasingly to improve water quality under the Clean Water Act [*Copeland*, 2006; *Berg et al.*, 2014]. Stream restoration strategies such as channel realignment [*Mason et al.*, 2012], riparian planting [*Roni et al.*, 2002], installation of in-stream structures [*Hester and Gooseff*, 2010; *Radspinner et al.*, 2010], and floodplain reconnection [*Opperman et al.*, 2009] help meet multiple restoration objectives (including improving water quality), although they are often installed with a single objective in mind.

Channel-spanning in-stream structures are a common feature of stream restoration projects, and include rock cross vanes [*Rosgen*, 2001; *Buchanan et al.*, 2012; *Daniluk et al.*, 2012; *Gordon et al.*, 2013], channel-spanning logs [*Sawyer et al.*, 2011; *Sawyer and Cardenas*, 2012], and steps [*Chin et al.*, 2009; *Endreny et al.*, 2011a]. In-stream structures are typically installed for bed stabilization or habitat creation [*FISRWG*, 1998; *Rosgen*, 2001]. They also create drops in the water surface, which induce hyporheic flow where short flow paths leave and return to the surface stream [*Wondzell and Swanson*, 1996; *Lautz and Siegel*, 2006; *Hester and Doyle*, 2008; *Wondzell*, 2011; *Ward et al.*, 2012]. Such structure-induced "hyporheic flow cells" augment similar exchange zones that occur naturally due to meander bends [*Boano et al.*, 2006], pool-riffle sequences [*Storey et al.*, 2003], and turbulence over coarse substrate [*Nagaoka and Ohgaki*, 1990]. Hyporheic zones have been much discussed for their promise of water quality benefits [*Hester and Gooseff*, 2010]. They create benthic or hyporheic habitat, cycle nutrients, attenuate pollutants, and moderate temperature—all of which can improve the ecological health of a stream [*Brunke and Gonser*, 1997]. Potential water quality improvements (e.g., denitrification) due to hyporheic flow are of particular interest for this study, though the hyporheic zone can act as either a source or a sink of pollutants [*Creswell et al*., 2008; *Zarnetske et al*., 2011].

Inset floodplains (also known as in-channel benches, two-stage channels, berms, and incipient floodplains) are narrow floodplain benches at some elevation above the channel bed but below the bankfull floodplain [*Royall et al*., 2010]. Inset floodplains form naturally when streams are recovering from extreme bank erosion linked to high flood frequencies [*Royall et al*., 2010] and are typically implemented by designers where channel incision or floodplain sedimentation causes bankfull floodplains to be inundated infrequently. Unlike bankfull floodplains that are typically inundated annually or biannually [*Soar and Thorne*, 2011], inset floodplains are inundated several times during the course of the year. Bankfull floodplains act as either sources or sinks of pollutants (e.g., excess nitrate and phosphorous) for short duration floods [*Haycock and Burt*, 1993; *Noe and Hupp*, 2007; *Heeren et al*., 2011]. Relatively few studies have investigated pollutant removal due specifically to inset floodplains although they have been found to retain organic material [*Changxing et al*., 1999; *Thoms and Olley*, 2004]. Pollutant removal may be expected from the settlement of contaminated soil particles (e.g., phosphorous) due to reduced velocity on floodplains [*Noe and Hupp*, 2009]. Inset floodplains also increase residence times of water (and therefore dissolved solute) relative to the channel, and increase surface area where denitrifying microbes can grow at or below the surface water-groundwater interface (benthic zone) [*Böhlke et al*., 2004]. For example, microbial denitrification rates from the top 5 cm of the soil from inset floodplains ranged from 0.02 to 6.7 mg N_2O–N m^{-2} h^{-1} for a first-order stream in Indiana [*Roley et al*., 2012b, 2012a].

1.2. Effects of Multiple Techniques on Solute Retention and Water Quality

A few studies have observed the effects of complementary stream restoration practices, including the effects of riparian vegetation and baffles [*Ensign and Doyle*, 2005], adding stream features (e.g., pools and riffles) and relocating a channel to its floodplain [*Bukaveckas*, 2007], different in-channel structures [*Hines and Hershey*, 2011], as well as a series of in-channel techniques and riparian wetland creation [*Filoso and Palmer*, 2011]. Other studies have observed how specific restoration design choices coupled with various environmental factors affect residence times or solute retention in the hyporheic zone [*Hester and Doyle*, 2008; *Sawyer et al*., 2011] or inset floodplains [*Roley et al*., 2012a]. Yet, the differences between in-stream structures and inset floodplains have not been analyzed to our knowledge. Clarifying and quantifying such differences between the effects of stream restoration practices is vital because stream restoration can be viewed by watershed managers as a single best management practice.

For significant reaction of channel-borne pollutants to occur, all reactants must be present [*Schnoor*, 1996], there must be a sufficient residence time [*Schnoor*, 1996; *Zarnetske et al*., 2011, 2012], and a sufficient proportion of streamflow must enter the retention zone (percent flow) [*Wondzell*, 2011]. The maximum pollutant reaction potential of a system can be assessed by analyzing solute retention (percent flow and residence time) and assuming all reactants are present. Pollution attenuation (e.g., denitrification) in river networks is typically concentrated in small streams [*Alexander et al*., 2000]. The fraction of streamflow entering the hyporheic zone is often limited by hydraulic conductivity [*Hester and Doyle*, 2008], although residence times are generally sufficient for reactions to occur [*Zarnetske et al*., 2011, 2012]. Neither the fraction of channel water traveling onto inset floodplains nor inset floodplain residence times have been analyzed previously.

A significant portion of pollutants travel downstream during stormflows [*Owens et al*., 1991; *Royer et al*., 2006], with some (e.g., phosphorous and fine sediment) moving downstream principally during stormflow, while others (e.g., nitrate) are transported more evenly between storm and nonstorm events [*Pionke et al*., 1999]. Stream restoration techniques will vary in their effects among these different flow regimes. Inset floodplains by definition are only activated during storms and are disengaged during most of the year. By contrast, in-stream structures lead to solute retention primarily during base flow [*Wondzell and Swanson*, 1996; *Ward et al*., 2012] by inducing hyporheic flow cells and in-channel backwater storage [*Ensign and Doyle*, 2005; *Hester and Doyle*, 2008]. Hyporheic zones have been shown to be effective at attenuating pollutants during base flow [*Kim et al*., 1995]. In-stream structures and inset floodplains may therefore complement each other in regards to when they are important (base flow versus stormflow), and what reaction condition they maximize (e.g., residence time or percent of streamflow entering retention zone).

1.3. Objectives of Study

The aim of this study was to compare hyporheic solute retention induced by in-stream structures with surface solute retention on inset floodplains. We numerically modeled surface water and groundwater hydraulics and coupled conservative tracer transport for a 90 m reach of Stroubles Creek in Blacksburg, Virginia. Our specific objectives were to determine how inset floodplain surface water solute retention and in-stream structure-induced hyporheic solute retention differ in terms of (1) when during the year they are active; (2) the proportion of streamflow expected to travel through the hyporheic zone or onto inset floodplains; (3) the residence times of water in these off-channel storage zones; and (4) the mass of solute stored in these zone. We analyzed these retention metrics while varying the restoration design parameters (e.g., inset floodplain length), geology, and hydraulic conditions.

2. Methods

2.1. Model Selection and Governing Equations

We used MIKE SHE, a finite difference integrated hydraulic model with coupled three-dimensional groundwater and two-dimensional surface water flow [*Graham and Butts*, 2005; *DHI*, 2011]. The groundwater component of MIKE SHE uses the groundwater flow equation:

$$\frac{\partial}{\partial x}\left(K_{xx}\frac{\partial h}{\partial x}\right)+\frac{\partial}{\partial y}\left(K_{yy}\frac{\partial h}{\partial y}\right)+\frac{\partial}{\partial z}\left(K_{zz}\frac{\partial h}{\partial z}\right)-Q=S\frac{\partial h}{\partial t} \tag{1}$$

where K_{xx} is the hydraulic conductivity in the *x* direction (m/s), K_{yy} is the hydraulic conductivity in the *y* direction (m/s), K_{zz} is the hydraulic conductivity in the *z* direction (m/s), h is the hydraulic head, Q is the source/sink term (m^3/s), and S is the storage coefficient (m^{-1}) [*DHI*, 2011]. MIKE SHE uses a fully implicit three-dimensional finite difference algorithm to solve the groundwater flow equation [*Graham and Butts*, 2005]. The surface water component of MIKE SHE uses the two-dimensional diffusive wave approximation of the Saint Venant equation solved using an explicit algorithm [*Graham and Butts*, 2005]. The full Saint Venant Equation in the downstream direction is:

$$\underset{(i)}{\frac{\partial u}{\partial t}}+\underset{(ii)}{u\frac{\partial u}{\partial x}}+\underset{(iii)}{g\frac{\partial h}{\partial x}}+\underset{(iv)\ (v)}{g(S_f-S_0)}=0 \tag{2}$$

where x is the distance in the downstream direction (m), u is the velocity component in the *x* direction (m/s), t is time (s), g is gravity (m/s^2), h is the depth of water (m), S_f is the slope of the energy grade line (dimensionless), and S_0 is the channel slope (dimensionless) [*Moussa and Bocquillon*, 2000; *Tsai*, 2005]. The terms above describe (i) local acceleration, (ii) convective acceleration, (iii) pressure gradient, (iv) friction, and (v) gravity. For the transverse direction, equation (2) is written in terms of y (the distance in the transverse direction) and v (the velocity in the y direction) instead of x and u, respectively [*DHI*, 2011].

The diffusive wave assumes that the local acceleration (i) and the convective acceleration (ii) can be disregarded, which is reasonable since the pressure gradient (iii) and the slope (v) are generally an order of magnitude larger than these terms [*Henderson*, 1966]. In this study, hydraulics were run to steady state so the local acceleration (i) is zero and only the convective acceleration (ii) is omitted. Generally, simplifications of Saint Venant Equation lead to similar results to the full equation but take less time to run [*Horritt and Bates*, 2001]. The diffusive wave simplification has been used successfully in various studies where overbank flooding occurs [*Hromadka et al.*, 1985; *Giammarco et al.*, 1996; *Weill et al.*, 2009].

Solute transport is modeled in both surface water and groundwater in MIKE SHE using the advection-dispersion equation:

Figure 1. Representative reach of Stroubles Creek showing main channel, inset floodplain, and bankfull floodplain. The approximate channel and inset floodplain widths used for modeling are also displayed. Photograph by W. C. Hession.

$$\frac{\partial c}{\partial t}=-\frac{\partial}{\partial x_i}(cV_i)+\frac{\partial}{\partial x_i}\left(D_{ij}\frac{\partial c}{\partial x_j}\right)+R_c \qquad i,j=x,y,z \tag{3}$$

where c is the concentration of tracer (g/m^3), V_i is the velocity tensor (m/s), D_{ij} is the dispersion coefficient (m^2/s), and R_c is the sum of the sources and sinks (g/m^3 s). Solute transport in saturated groundwater is modeled in the longitudinal (x), transverse (y), and vertical (z) directions. A uniform c within a cell is assumed for surface water solute transport, canceling out all vertical terms in equation (3).

2.2. Model Setup

2.2.1. Study Site

The study site is a 90 m long reach of a 1.5 km restored segment of Stroubles Creek, a third-order stream in Blacksburg Virginia. Physical, hydraulic, and hydrologic properties were based on this site and were the basis for scenario testing, although we did not perform model calibration or validation. The site is within the Stream Research, Education, and Management Lab (StREAM Lab, www.bse.vt.edu/site/streamlab/index.html) that has been monitored by the Virginia Tech Biological Systems Engineering Department since 2008 [*Thompson et al*., 2012]. The drainage area of the reach is approximately 15 km^2, with primarily urban and agricultural land use. Prior to restoration, inset floodplains were forming naturally at several meanders. As a result, inset floodplains were incorporated into the restoration design along with riparian zone planting and bank stabilization. Vegetation ranges from grasses to brush on the inset floodplains (Figure 1). Vegetation is primarily grasses on the bankfull floodplain along with saplings planted during the restoration. The main channel was designed to carry a natural bankfull event ($\sim$5.7 m^3/s) [*Keaton et al*., 2005], but since the watershed is heavily developed, the inset floodplain widths were designed to carry recently observed top-of-bank flows of $\sim$8.5 m^3/s [*Wynn et al*., 2010]. There are currently no in-stream structures present. We chose this location for our modeling study because (1) the drainage area was both urban and agricultural and was therefore a typical candidate for restoration [*FISRWG*, 1998], (2) both natural and constructed inset floodplains were present, and (3) hydrologic data were available for model development.

2.2.2. Model Domain and Computational Grid

We determined the location and extent of the model domain based on the geometry of Stroubles Creek and the availability of groundwater data. Restoration of 1.5 km of Stroubles was completed in early 2010, including inset floodplains along a 500 m reach [*Wynn et al*., 2010]. Within this reach there is a transect of six piezometer nests oriented perpendicularly to the channel with three nests extending east and three extending west (all are single-zone wells with 15 cm openings). We used water level data from the four piezometer nests closest to the stream to represent the groundwater conditions adjacent to the stream (B, C,

10.1002/2013WR014400

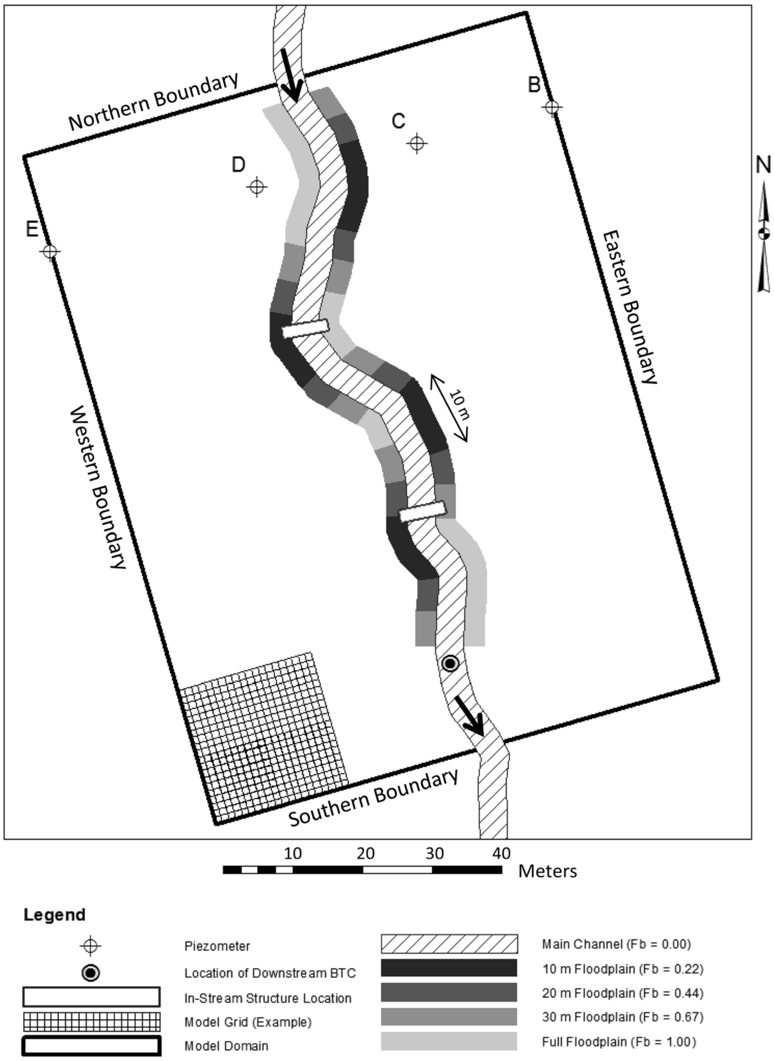

Figure 2. Inset floodplain location and extent for all floodplain scenarios modeled. The model grid is displayed for a portion of the model domain, and the location where the breakthrough tracer curve (BTC) is taken downstream of the inset floodplains is also shown. The size of the in-stream structures is exaggerated.

D, E in Figure 2). Each nest is composed of a shallow and a deep piezometer, although only the deep piezometers were used for this study because the water table was often below the shallow piezometers. There are intermittent water table data from this transect from 2010 to 2012, as well as approximately 1 year of continuous data in 2010. The model domain extended laterally (perpendicularly to the channel) out to the second piezometer nest away from the channel resulting in a model width of 75 m. This allowed hydraulic data from these piezometers to be used as boundary conditions. The longitudinal model domain length (100 m) was chosen to include a sufficient number of meanders for analysis of inset floodplains (four).

The grid discretization (1 m by 1 m) was selected as a compromise between model run time and a grid resolution fine enough to adequately simulate structure-induced hyporheic flow and produce a relatively smooth channel bed. The horizontal pattern of groundwater and surface water grids in MIKE SHE must be identical [*DHI*, 2011], so both the surface water and groundwater grid were 1 m^2 in the horizontal directions. The surface water transport portion of the model was always the limiting factor for run times, and thus minimum possible surface water grid sizes were also used in the groundwater domain. Model run times were several days at this resolution, and increased to over a week with a 0.5 m to 0.5 m grid which often caused model or computer failure. In sum, this grid configuration was the only one that would allow us to address our research objectives. With this grid resolution there were 102 rows, 77 columns, and 7850 cells.

Layer thickness in the groundwater model domain was uniform in the vertical dimension but varied horizontally. The groundwater layer thickness below the thalweg was set to 0.2 m. The lower extent of the groundwater domain (5 m below the thalweg) was selected so that hyporheic flow was not affected by the no-flow boundary at the bottom of the model domain. The number of vertical layers (25) was held constant horizontally throughout the model domain such that the layers were thicker beneath the bankfull floodplain than beneath the channel.

2.2.3. Topography and Bathymetry, Including Inset Floodplains

We derived surface topography from seven stream cross sections surveyed in 2012 superimposed over a LIDAR elevation grid from 2009 (prerestoration). The points were converted to a raster in ArcGIS, then imported and interpolated to a 1 m by 1 m MIKE SHE elevation grid file. Inset floodplains were surveyed at the restored reach of Stroubles Creek during the summer of 2012 using a Johnson Level and Tool electronic self-leveling horizontal rotary laser level (40–6535). Seven transects were surveyed at approximately 50 m intervals down the channel, with elevations measured at a maximum of 2 m horizontal intervals along the transects. The thalweg as well as the edges of bankfull floodplains, inset floodplains, and the channel were also surveyed at each transect.

To help generalize our results, we created a simplified channel-floodplain cross section by taking the averages of key geometric parameters from the seven surveyed cross sections. The channel top width used for modeling was 3.5 m, the inset floodplain width was 3.0 m (Figure 1), and the slope from the inset floodplain to the bankfull floodplain was 3:1 (horizontal: vertical). The bottom of the channel had a triangular cross section that was 1.7 m wide and 0.15 m high. The average longitudinal channel slope of 0.0023 m/m was calculated from a 2011 StREAM Lab survey. Using an average slope removes pools and riffles where natural hyporheic flow is expected. However, because this study focused on the effects of in-stream restoration structures on hyporheic exchange, this simplification is appropriate. The prerestoration "incised" bank slope (1:1.25) was used where inset floodplains were not present and was estimated from a 2009 StREAM Lab stream survey. Elevation grids were created such that the inset floodplains were centered at meander apexes, and 0, 10, 20, and 30 m in length (Figure 2). We also created a full inset floodplain scenario that extended as far as the most downstream and upstream segments of the 30 m inset floodplains on both banks without any breaks (the length for this scenario is 90 m). Inset floodplain lengths were generalized by calculating

$$F_b = \frac{L_{FP}}{L_B} \tag{4}$$

where F_b is the fraction of bank with inset floodplain (m/m), L_{FP} is the total length of inset floodplain added (m), and L_B is the total length of stream bank (m). The five different floodplain scenarios discussed above correspond to F_b of 0.00, 0.22, 0.44, 0.67, and 1.0, respectively. We superimposed the simplified cross sections over the LIDAR grid creating grid files with the existing LIDAR-derived topography overlaid with the interpolated channel for each of the inset floodplain scenarios.

2.2.4. Surface Water Properties

There are three physical inputs for modeling surface water hydraulics and solute transport in MIKE SHE: Manning's roughness coefficient (n), the transverse dispersion coefficient (ε_t), and the longitudinal dispersion coefficient [*DHI*, 2011]. We estimated n using the methods outlined by *McCuen* [2005] for the main channel and from *Arcement and Schneider* [1989] for the inset floodplain. Both methods are based on channel and floodplain properties (i.e., regularity of channel, flow obstructions, variation of x sections, vegetation, and degree of meandering). GIS was used to calculate the sinuosity, and a field inspection was used to estimate the remaining parameters. The channel n used for modeling was 0.03 and the inset floodplain n during the summer was 0.07. We conducted a sensitivity analysis to confirm that varying n from our assumed values did not affect our conclusions (see section 4).

We estimated ε_t in the field using the method outlined by *Fischer* [1973] for side discharge of a conservative visual tracer (i.e., suspended silt particles) using

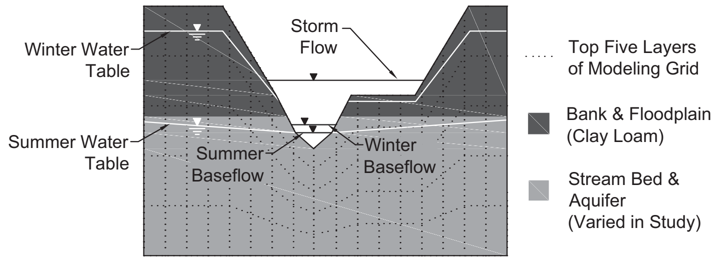

Figure 3. Conceptual diagram of hydrological conditions and soil/sediment texture used in model with five upper model layers shown. When multiple soil/sediment textures are present in a single cell, a weighted average is calculated for all hydraulic properties.

$$L = \frac{0.4\,\bar{u}\,W^2}{\varepsilon_t} \tag{5}$$

where L is the mixing length (m), $\bar{u}$ is the average stream velocity (m/s), W is the channel width (m), and ε_t is the dispersion coefficient in the transverse direction (m^2/s). We estimated the mixing length at 14 m, corresponding to a ε_t of 0.04 m^2/s, consistent with other field studies [*Fischer*, 1973; *Fischer et al*., 1979]. We conducted a sensitivity analysis to confirm that varying ε_t from our assumed values did not significantly affect our conclusions (see section 4). When considering longitudinal mixing, the effects of advection and longitudinal dispersion are additive [*Fischer et al*., 1979]. Since advective mixing is approximately 40 times larger than longitudinal dispersion [*Fischer et al*., 1979], a longitudinal dispersion coefficient of 0 was used.

2.2.5. Soil/Sediment Properties

We used two porous media textures in the model: clay loam (bank and floodplain soil) and silty-gravel (streambed and aquifer**,** Figure 3). We selected values for hydraulic conductivity (K) from StREAM Lab field slug tests performed in the summer of 2009 and from the accepted literature values [*Holtz and Kovacs*, 1981; *Anderson and Woessner*, 1992] (Table 1). We set the base case streambed and aquifer K to 1×10^{-6} m/s. The location of the border between the two soil types was based on StREAM Lab soil borings, and cells that included both soil types used a weighted average to calculate hydraulic properties. We varied the K of the streambed and aquifer from that representative of silty-clay (1×10^{-8} m/s) to coarse sand (1×10^{-4} m/s) [*Holtz and Kovacs*, 1981; *Anderson and Woessner*, 1992]. This represented urban and agricultural streams where fine sediments are prevalent [*Wood and Armitage*, 1997; *Calver*, 2005]. We assumed the streambed was homogeneous and isotropic, but acknowledge that soil in natural systems is typically heterogeneous with preferential flow [*Cardenas et al*., 2004], including flow through macropores [*Menichino et al*., 2014]. We did not vary the K of the bank and floodplain soil. We used accepted values from the literature for porosity, specific yield, and specific storage [*Freeze and Cherry*, 1979; *Holtz and Kovacs*, 1981; *Anderson and Woessner*, 1992]. Groundwater hydrodynamic dispersivities were set to representative values for local dispersivity from the literature (Table 1) [*Gelhar et al*., 1992; *Cirpka et al*., 1999; *Cirpka and Kitanidis*, 2000; *Sawyer and Cardenas*, 2012].

2.2.6. Boundary Conditions

All hydraulic boundary conditions were held constant (steady state) for both the surface water and groundwater components of the system. For the groundwater portion of the model domain, we used a no-flow boundary at the lower extent of the domain, and fixed head boundaries along the northern, southern, eastern, and western boundaries (Figure 2). We used two sets of groundwater fixed head boundary conditions for this study, a summer steady state condition and a winter steady state condition. Both conditions were estimated from StREAM Lab piezometer data from 2009 to 2012 (Table 2). During the summer of 2009, a second piezometer transect was monitored 120 m downstream of the transect used for this study with

Table 1. Summary of Base Case Soil Property Values Used for Hydraulic and Solute Transport Modeling

Description	Bank and Floodplain	Streambed and Aquifer
Soil type	Clay loam	Silty gravel
Hydraulic conductivity (K) (m/s)	1×10^{-8}	1×10^{-6}
Porosity	0.49	0.30
Specific storage (1/m)	0.001	0.0005
Specific yield	0.13	0.20
Longitudinal dispersivity (m)	0.01	0.01
Transverse dispersivity (m)	0.001	0.001

Table 2. Approximate Average Steady State Summer and Winter Water Table Depths for Active Piezometers

Piezometer	Depth of Water Table Below Ground Surface (m) Winter	Summer
B	0	1
C	0	1.2
D	0.5	1.4
E	0.2	1.3

approximately the same orientation and spacing. There was variation in the water table depth below the ground surface from one transect to the next for the inner piezometers (i.e., piezometers C and D in Figure 2) of up to 1.3 m, while the variation in depth below the ground surface for the outer piezometers (i.e., piezometers B and E in Figure 2) was less than 0.4 m during the period of record. As a result, for the eastern and western boundaries we assumed the water table was located at a constant depth below the ground surface. In particular, we used the water table depths measured at piezometers B and E, respectively, and varied the groundwater table elevation based on the topography. For the northern fixed head boundary, we linearly interpolated the groundwater table using the water depth below ground surface at piezometers B, C, D, and E and the stream level. For the southern boundary, we only used the depth below ground surface indicated by the outer piezometers (i.e., B and E) and the stream level to interpolate the groundwater table elevation.

The surface water flow component of the model required specified stages at the upstream and downstream boundaries. A StREAM Lab stream gage is located 300 m upstream of the study site without any significant tributaries in between. Three steady state stages were estimated using continuous data collected at this gage from May 2011 to May 2012: summer base flow (flow depth of 0.1 m in the channel), winter base flow (depth of 0.15 m), and stormflow (depth of 0.65 m). For the storm stage, we selected the median of all inset floodplain activating stages (depth $>$ 0.5 m) over the course of the gaging period. The existing site is closest to the scenario with inset floodplain lengths of 20 m ($F_b = 0.44$) with no in-stream structures, so we used this case to calculate channel discharges by inputting each of the three steady state stages as boundary conditions. Using this method, we found that the streamflows for summer base flow, winter base flow, and stormflow were 0.025, 0.059, and 1.7 m^3/s, respectively. These flows were held constant for all additional model runs by adjusting the surface water boundary stage. These flows matched the existing stage-storage relationship at Stroubles Creek reasonably well, although a rigorous analysis was not performed due to the conceptual nature of this study.

We combined these surface water boundary conditions with the groundwater boundary conditions to produce three steady state sets of overall hydraulic boundary conditions (Figure 3). These scenarios were (1) a summer base flow scenario (summer base flow with summer groundwater), (2) a winter base flow scenario (winter base flow with winter groundwater), and (3) a stormflow scenario (stormflow with summer groundwater). During the storm scenario, steady state surface water boundary conditions represent peak flows during storms and steady state groundwater conditions represent situations where stormflows come from upstream in the channel with an absence of local precipitation to raise hillslope groundwater levels. Although unsaturated (vadose) zone processes were not modeled, during stormflow scenarios channel water flowed onto the inset floodplains, which were situated over the unsaturated zone (Figure 3). In these situations, MIKE SHE uses Darcy's law to calculate the recharge from surface water to the saturated zone. However, since the floodplain sediment is fine ($K = 1 \times 10^{-8}$ m/s) this recharge had a negligible effect on the saturated zone over a storm duration. Hydraulic model mass balance errors were less than 0.2% for all model runs.

For solute transport, we input a conservative tracer at the upstream surface water boundary (northern model boundary) with a constant concentration of 1 g/m^3 (Figure 2). The tracer was only added once the hydraulic model had reached steady state. We used a step tracer increase for all solute tracer analyses, and turned the tracer loading off after 10 min for stormflow scenarios to better visualize tailing effects due to inset floodplains. We did not turn the tracer loading off for summer base flow (i.e., when the hyporheic zone is engaged) because it took much longer to reach a steady state concentration.

2.2.7. In-Stream Structure Geometry

We based the geometry and spacing of in-stream structures on the literature data, model grid constraints, and physical constraints. Spacing for in-stream structures typically varies from 10 to 200 m and scales with stream discharge [*Radspinner et al.*, 2010]. We calculated structure spacing for this study from cross vane

Table 3. Parameters Varied for Sensitivity Analysis

Parameter	Description	Base Case	Minimum	Maximum	Presence of Structures
Surface and groundwater hydraulic boundaries	1. Summer base flow 2. Winter base flow 3. Stormflow	Summer base flow	NA	NA	Run both with and without
Streambed and aquifer sediment hydraulic conductivity (K)	Varied from that of a coarse sand to a silty–clay	1×10^{-6} m/s	1×10^{-8} m/s	1×10^{-4} m/s	Run with structures only
Inset floodplain length	Length of individual inset floodplain segment	20 m ($F_b = 0.44$)	0 m ($F_b = 0.00$)	90 m ($F_b = 1.0$)	Run with structures only[a]

[a]When varying the surface and groundwater hydraulic boundaries, the stormflow scenario was run with and without structures for the base case inset floodplain length (20 m). No effect was observed, so the analyses varying the floodplain length were only run with structures present. NA = not applicable.

spacing from two studies with similar drainage areas to Stroubles Creek, scaled by discharge. The cross vane spacing was approximately 100 m [*Buchanan et al*., 2012] and 150 m [*Crispell and Endreny*, 2009] for streams with base flow discharge of 0.2 m^3/s (estimated from USGS gaging station near Bethel Grove, NY) and 0.05 m^3/s [*Crispell and Endreny*, 2009], respectively. For a summer base flow of 0.025 m^3/s at Stroubles Creek this scaled to a spacing of approximately 15–75 m, with average of 45 m. This translates to two in-stream structures over our 90 m reach where inset floodplain variation occurred. We used the 90 m reach instead of the full reach so solute retention could be directly compared between inset floodplains and in-stream structures.

The length of the in-stream structures (in the direction of channel flow) was 1 m due to the model grid resolution, and the width of the structures (perpendicular to channel flow) varied depending on how channel geometry intersected the square grid cells (2 or 3 m). We set the height of the structures (0.3 m) using the methodology outlined by *Rosgen* [2001] that calculates the structure height based on the slope of the cross vane arm from the bank to the channel. It is possible for in-stream structures to be partially submerged on the downstream side due to other structures or geometric features [*Chin*, 2003; *Anderson et al*., 2005]. The in-stream structure geometry and spacing used for this study resulted in such a partially submerged condition for the upstream structure but not the downstream one. The modeled structures therefore together represent the range of possible conditions expected to occur. A vane slope of 4.5% (average of the 2–7% range specified by *Rosgen* [2001]) was used. The in-stream structures are located where inset floodplains are present to avoid additional negative impacts of construction activities [*FISRWG*, 1998], and because 4.5% slope from the prerestoration bank to the channel would lead to unrealistic structure heights (i.e., $>$0.5 m) based on the geometry of Stroubles Creek [*Radspinner et al*., 2010; *Wynn et al*., 2010]. There is considerable variability in whether modeling studies do [*Endreny et al*., 2011a, 2011b] or do not [*Lautz and Siegel*, 2006; *Hester and Doyle*, 2008] extend the impervious part of the in-stream structure down into the sediment. For this study, the structures extended one computational layer ($\sim$0.2 m) into the subsurface.

2.2.8. Sensitivity Analysis

We performed a total of 14 model runs varying the hydraulic boundaries, hydraulic conductivity, inset floodplain length, and the presence of structures (Table 3). For each of these model runs, we used the n and ε_t estimated in the field. An analysis on the effect of n and ε_t on our results is available as supporting information. We also performed additional sensitivity analyses on groundwater level (for summer base flow stream stage), and the stream stage (for summer base flow groundwater levels).

2.3. Modeling Output

2.3.1. Flow and Storage

We separated the surface water domain into two distinct components (main channel and inset floodplain) and the groundwater into two components (hyporheic and nonhyporheic). The inset floodplains were delineated based on the depth of water during stormflow, with the exception of cells where the majority of the water flowing onto a floodplain cell immediately flowed back onto the channel (i.e., 90% of the flow onto the inset floodplain immediately left again). With this delineation, the flow onto and off of the floodplains could be calculated using MIKE SHE flow output, and the volume could be calculated in the main channel and inset floodplain using the depth results. The solute mass on the inset floodplain and in the main channel was calculated similarly by multiplying the volume of water in each cell by its concentration of tracer. For the purposes of this analysis, we considered the mass of solute located on the inset floodplains to be storage (albeit for short periods of time).

Given the gaining nature of the reach, we considered all groundwater cells with greater than 10% concentration of conservative tracer to be potentially hyporheic [*Lautz and Siegel*, 2006], and double checked this delineation approach using particle tracking. Ten particles were added to any groundwater cell that was potentially hyporheic, and if any of those particles entered the channel downstream of the in-stream structures, the cells were considered hyporheic and were included for volume and mass calculations. The mass of solute in groundwater cells was calculated as the product of the porosity, cell volume, and concentration of solute tracer. In-stream structure-induced hyporheic flow was calculated by summing the flow for all hyporheic cells (as defined above) downstream of the in-stream structures (i.e., the upwelling portion of the hyporheic flow cells).

2.3.2. Residence Time

We exported conservative tracer breakthrough curves from the transport model to analyze solute moving in surface water (i.e., in the channel and on the inset floodplains) and in groundwater (upwelling portion of hyporheic flow cells). The time to 50%, 75%, and 99% of the steady state concentrations (i.e., t_{50}, t_{75}, and t_{99}) were calculated from the breakthrough curves, and were used to estimate residence times. We calculated t_{50}, t_{75}, and t_{99} in the main channel 2 m downstream of the downstream end of the full inset floodplain to approximate full reach residence times (Figure 2) and also at equally spaced intervals along the channel. The reach residence time enhancement ratio due to the storage (RT_{ER}) was calculated by dividing the residence times for a given F_b by the residence time when $F_b = 0$. If adding inset floodplain segments had no effect on the residence time the RT_{ER} would be 1, and if adding inset floodplain segments doubled the residence time the RT_{ER} would be 2. The t_{50} was also calculated for the main channel for summer and winter base flow scenarios to quantify surface storage due in-stream structures.

We calculated residence times on individual inset floodplains and within in-stream structure-induced hyporheic flow cells using breakthrough curves at locations representing the center of solute mass flux exiting the storage zones and returning to the channel. The total mass flux leaving an inset floodplain was calculated by multiplying cell tracer concentrations by flow leaving each cell and summing. The same methods were used to calculate the mass flux in the hyporheic zone with the additional step of multiplying the result by the porosity. The location of the cell at the center of solute mass flux exiting each storage zone was found by tracking the mass flux for each cell along a storage zone boundary and comparing it to the total storage zone mass flux.

2.3.3. Fraction of Year That Storage Occurs

We estimated the portion of the year when in-stream structure-induced hyporheic flow is expected at Stroubles Creek by performing a sensitivity analysis on the groundwater levels for summer base flow scenarios. The groundwater level was used as an indicator of the degree of gaining of the stream due to the availability of groundwater data. We performed this sensitivity analysis because the degree of gaining is the strongest controlling variable for determining whether hyporheic flow will occur or not [*Cardenas and Wilson*, 2006; *Lautz and Siegel*, 2006; *Hester and Doyle*, 2008; *Sawyer and Cardenas*, 2012]. We then calculated what percent of the year the groundwater levels were within the levels where hyporheic flow was expected.

We performed an additional sensitivity analysis on the base flow stream stage. We did this to estimate the stream stages when surface storage due to in-stream structures was expected. We estimated the portion of the year where inset floodplains were active by calculating the total time that the stream stage measured at the stream gage exceeded the inset floodplain elevation (0.5 m).

2.3.4. Scaling Equations

We derived a simple empirical equation to estimate the scaling effect between K and the fraction of streamflow that enters the in-stream structure-induced hyporheic zone:

$$Q_{F\text{-}HZ} = \frac{(9.2\times10^{-3})KL_R}{Q_{CHANNEL}} \tag{6}$$

where $Q_{F\text{-}HZ}$ is the fraction of streamflow that flows through the in-stream structure-induced hyporheic zone (dimensionless), $Q_{CHANNEL}$ is surface water flow in the channel (m^3/s), K is the hydraulic conductivity (m/s), and L_R is the length of restored reach (m) with two 0.3 m in-stream structures every 90 m, all for summer base flow conditions at Stroubles Creek. Equation (6) can be written more generally as:

$$Q_{F\text{-}HZ} = \frac{(\gamma K) D_s L_R}{Q_{CHANNEL}} \tag{7}$$

where γ is a hyporheic hydraulic coefficient (m^2), D_s is the structure density (m^{-1}), and L_R is the length of restored reach with in-stream structure density D_s (m). For this study γ is 0.41 m^2 (from linear regression), D_s is 2/90 m^{-1}, L_R is 90 m, and $Q_{CHANNEL}$ is 0.025 m^3/s.

A simple scaling equation was also derived for the RT_{ER} with varying F_b:

$$RT_{ER} = 1 + L_R \beta \tag{8}$$

$$\beta = \begin{cases} 0.0018(F_b) & \text{if } F_b \leq 0.67 \\ (0.0018)(0.67) - 0.0002(F_b - 0.67) & \text{if } F_b > 0.67 \end{cases} \tag{9}$$

where RT_{ER} is the reach residence time enhancement ratio due to inset floodplain installation (dimensionless), L_R is the length of reach where restoration takes place (m), β is the inset floodplain-main channel exchange coefficient (m^{-1}) defined by equation (9), and F_b is the fraction of bank with inset floodplains.

3. Results

3.1. Exchange Flows With Storage Zones

For stormflow scenarios, water primarily flowed from the main channel onto the inset floodplains within the upstream half of their shared boundary, and from the floodplain back into the channel within the downstream half (Figure 4). The fraction of channel flow that flowed onto the inset floodplains ($Q_{F\text{-}FP}$) across the entire reach increased nonlinearly with fraction of bank with inset floodplain (F_b, Figure 5). $Q_{F\text{-}FP}$ plateaued when F_b was 0.67 (individual inset floodplain length of 30 m) with approximately 56% of the channel flow spending some time on the floodplains. During summer and winter base flow scenarios there was no surface water flow onto the inset floodplains (as expected).

Stroubles Creek was gaining during base flow scenarios in both the summer (Figure 6a) and winter (Figure 6b), but was more gaining in the winter due to higher groundwater levels. In-stream structure-induced hyporheic flow occurred in summer but not in winter due to these differences in background groundwater levels. There was no structure-induced hyporheic flow in winter, although the magnitude of upwelling directly upstream of the structures decreased and the magnitude of upwelling directly downstream of the structures increased relative to when no structures were present. The magnitude of hyporheic flow for the downstream structure was larger than that of the upstream structure due to the larger head drop across the structure (Figure 6c). This difference in head drop was in turn due to the upstream structure being partially submerged by the backwater from the downstream structure. During stormflow the stream was generally losing, and the water depths in the channel upstream and downstream of in-stream structures were the same such that in-stream structure-induced hyporheic flow did not occur. As anticipated by Darcy's law there was a linear increase ($R^2 = 1.00$) in the fraction of channel flow that entered the in-stream structure-induced hyporheic zone ($Q_{F\text{-}HZ}$) as hydraulic conductivity (K) increased for the summer base flow scenarios ($Q_{F\text{-}HZ}$ of 0.00003–0.003 for K of 1×10^{-8} to 1×10^{-4} m/s). We used linear regression of these results ($Q_{F\text{-}HZ}$ versus K, not shown) to calculate the regression coefficient used for equation (6).

3.2. Mass Storage

The mass of solute present on the inset floodplains increased with F_b, with a slight decrease in slope as F_b approached 1.0 (Figure 5). We used the ratio of solute mass in the main channel to that present on the inset floodplain to illustrate how the mass of solute on the floodplain compares to that in the channel. Less mass was stored on the floodplains than was located in the channel for all F_b, with the mass on the floodplains for $F_b = 1.0$ (full inset floodplain) approaching 50%. For the stormflow scenario, the solute concentration

10.1002/2013WR014400

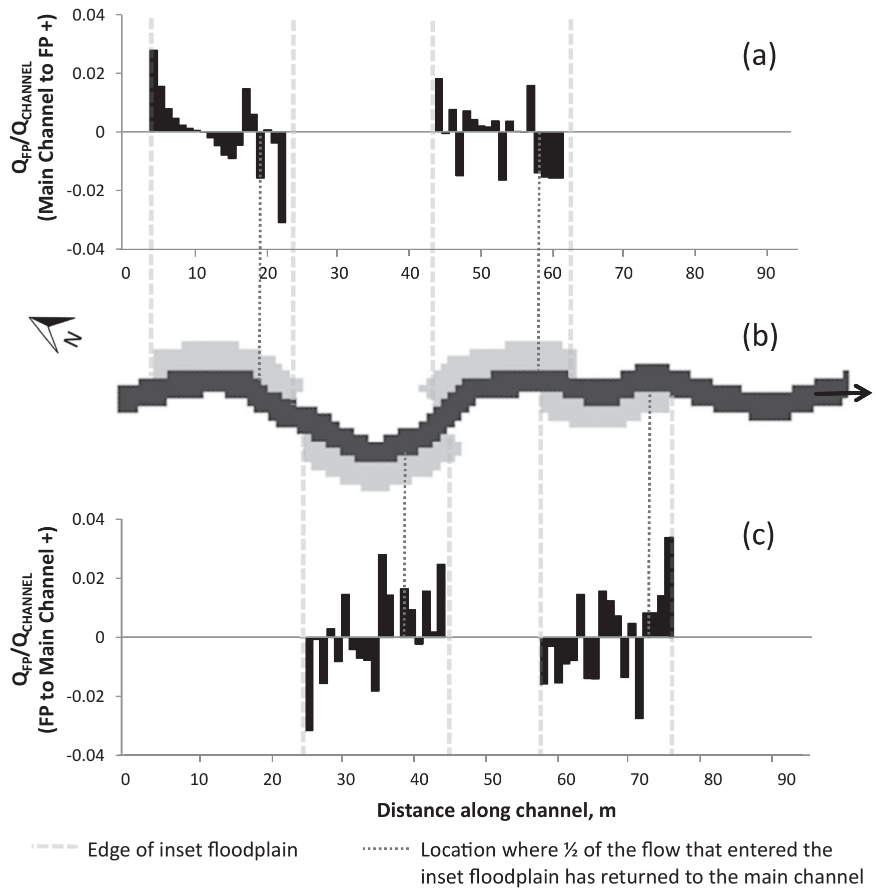

Figure 4. Exchange flow between main channel and area above inset floodplains (Q_{FP}) normalized by the channel flow at the upstream boundary ($Q_{CHANNEL}$) versus longitudinal distance along stream for the (a) east bank and (c) west bank for stormflow scenario. (b) The digitized main channel of Stroubles (dark gray) and inset floodplains (light gray) are also displayed. To make the direction of flow more visually intuitive, *y* axes of plots in Figures 4a and 4c are reversed such that flow out of the channel onto the floodplain is positive in Figure 4a and negative in Figure 4c. This causes all flow moving east across the main channel-inset floodplain boundary to be displayed as positive, and all flow moving west to be displayed as negative.

present everywhere on the floodplains is the same as the upstream boundary condition (1 g/m^3). As a result, the mass of solute stored on the inset floodplains normalized by the mass of solute stored within the main channel is nearly identical to the floodplain water volume storage normalized by main channel volume.

For summer base flow scenarios at steady state hydraulic and transport conditions, there was 3.9 times more water (by volume) and 2.8 times more mass of solute stored in the structure-induced hyporheic zone than in the channel. The length and width of these two hyporheic flow cells were largest at the uppermost groundwater layer (up to 20 m long and 7 m wide) and decreased with depth. Although

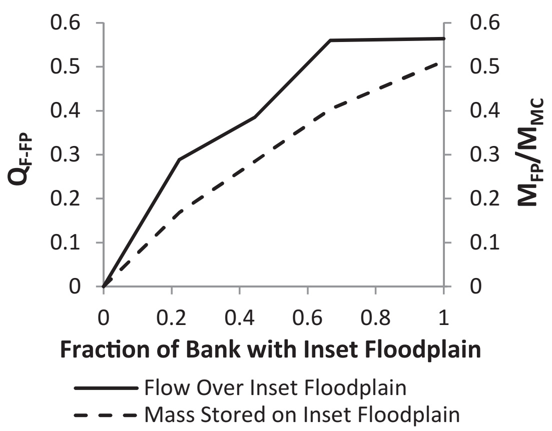

Figure 5. Fraction of surface water flow that flowed onto inset floodplains ($Q_{F\text{-}FP}$) and total mass stored on inset floodplains (M_{FP}) normalized by the mass of solute in the main channel (M_{MC}) versus fraction of bank with inset floodplain (F_b). Both $Q_{F\text{-}FP}$ and M_{FP}/M_{MC} are for stormflow scenarios.

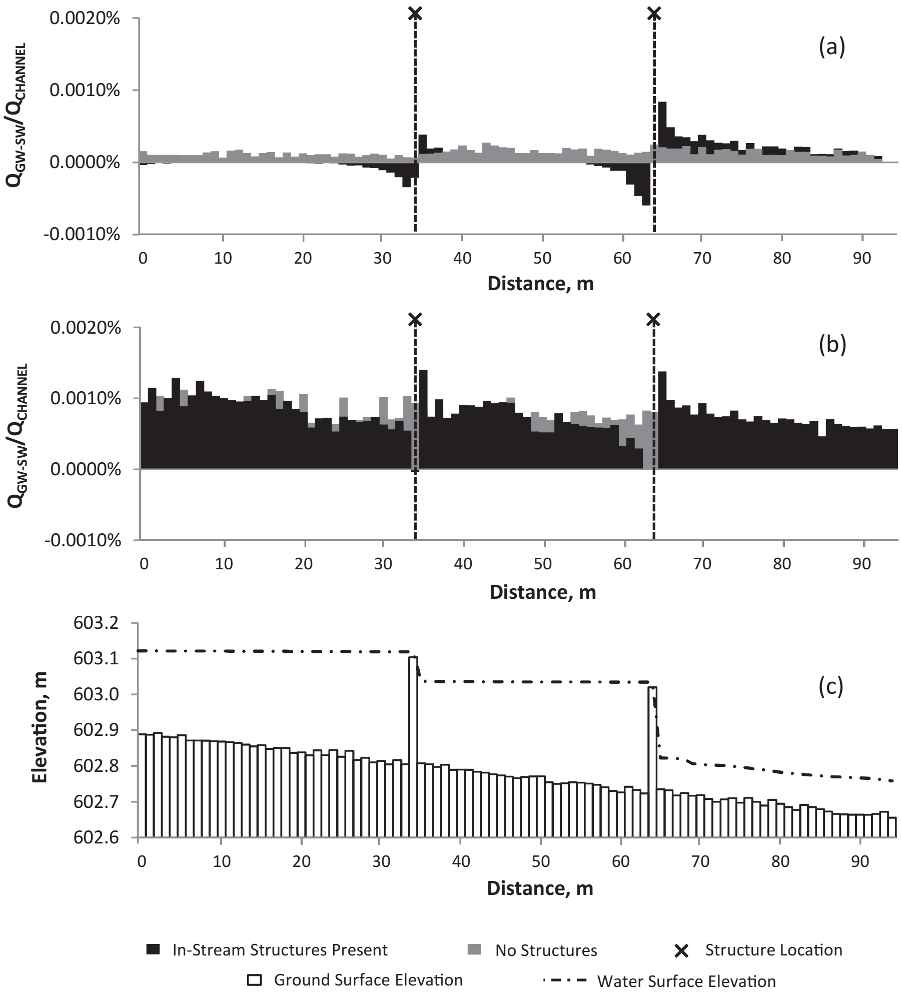

Figure 6. Flow from groundwater to stream channel (Q_{GW-SW}) normalized by the channel flow at the upstream boundary ($Q_{CHANNEL}$) versus longitudinal distance along channel for (a) summer base flow and in (b) winter base flow scenarios. (c) The ground surface elevation and water surface elevation for summer base flow are also displayed.

hyporheic residence times are high, hyporheic flow does not exist at certain times of year (e.g., winter), and storm events periodically interrupt hyporheic exchange. For these reasons, actual storage in the hyporheic zone is generally expected to be less than this theoretical steady state summer maximum, and increases with duration of base flow conditions. For example, when the duration of summer base flow increased from 10 to 60 days, the mass of tracer stored in the in-stream structure-induced hyporheic zone more than doubled.

3.3. Residence Times

Channel residence times in the modeled reach were longest for summer base flow scenarios and shortest for stormflow scenarios (Figure 7a). Residence times increased in the presence of structures during summer and winter base flow scenarios but did not for the stormflow scenario. The largest change in median residence time due to adding structures occurred for summer base flow (factor of 3), followed by winter base flow (factor of 2).

During storms, the time to reach a steady state concentration at the downstream location (and return to baseline) increased as inset floodplains were added and as F_b increased (Figure 7b). The upper end of the residence time distribution was most affected. The reach residence time enhancement ratio (RT_{ER}) for the time to 50%, 75%, and 99% of the steady state concentrations (i.e., t_{50}, t_{75}, and t_{99}) increased relative to

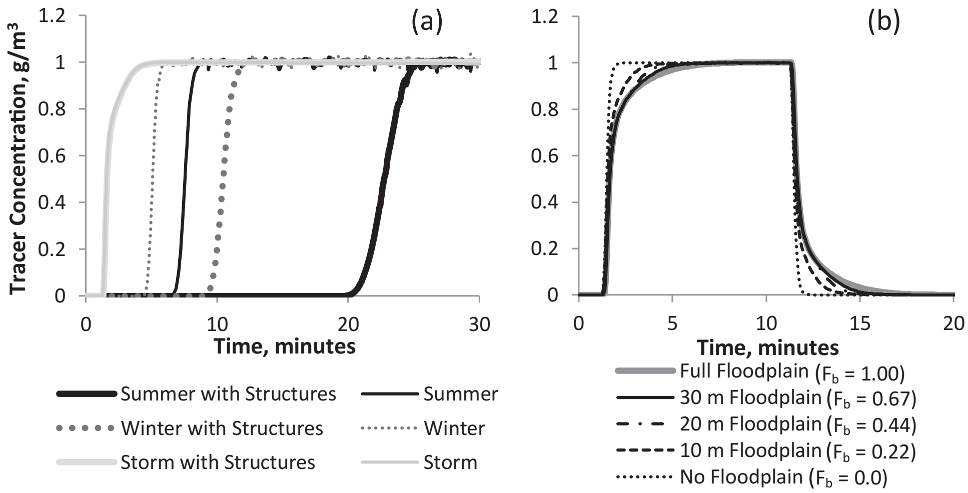

Figure 7. (a) Conservative tracer breakthrough curves in the thalweg at the downstream model boundary for summer base flow, winter base flow, and stormflow scenarios with and without structures. For all scenarios displayed, the fraction of bank with inset floodplains (F_b) is 0.44. (b) Breakthrough tracer curves at the same location are also shown for the stormflow scenario with varying F_b.

when no floodplains were present (Figure 8). t_{99} linearly increased with F_b, while both the t_{50} and t_{75} leveled off at $F_b = 0.67$ and $F_b = 0.44$, respectively.

The t_{50} RT_{ER} from adding inset floodplains increased with distance along the channel (e.g., for $F_b = 0.67$ the RT_{ER} after 25 feet was 1.02 and after 75 feet was 1.1). The increase in RT_{ER} when traveling downstream was generally linear ($0.94 < R^2 < 0.97$, not shown) with slight undulations associated with the complex flow behavior of the floodplains as well as their locations along the stream. The RT_{ER} also increased with F_b for values of F_b from 0.00 to 0.67. The RT_{ER} for $F_b = 0.67$ is greater than the RT_{ER} for $F_b = 1.0$ at some locations along the channel and it is less in others. We used linear regression of these results (RT_{ER} versus distance downstream) to calculate the regression coefficient used for equations (8) and (9). We used the β term to account for the nonlinear increase in slope with F_b.

We also evaluated residence times on individual inset floodplains. We calculated the center of mass flux exiting the floodplain by locating where half of the total mass flux that flowed onto an inset floodplain segment had exited the inset floodplain and reentered the channel (Figure 4). For an inset floodplain length of 20 m ($F_b = 0.44$), the center of mass flux exiting each individual inset floodplain was located between 70% and 90% of the floodplain length downstream from the upstream end of the floodplain (Figure 4). This percentage varied for other inset floodplain lengths, but was always between 60% and 90%. As the inset floodplain length (and consequently F_b) increased, it took longer for steady state solute concentrations to be reached at the center of mass flux exiting the floodplain (Figure 9a). Compared to the location of the center of mass flux leaving the floodplain, breakthrough tracer curves toward the start of the floodplains were steeper and reached steady state faster, while those toward the end were less steep and reached steady state slower (not shown). Breakthrough tracer curves shown in Figure 9a are for the northernmost inset floodplain segment so the effect of travel time in the channel is minimized. Nevertheless, to more accurately estimate inset floodplain residence

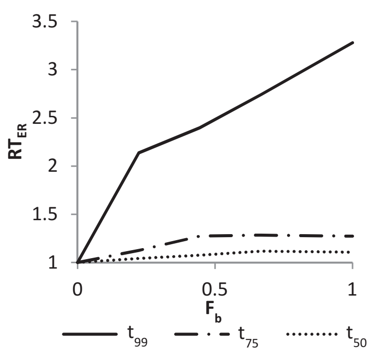

Figure 8. Reach residence time enhancement ratio (RT_{ER}) versus fraction of bank with inset floodplain (F_b) for stormflow scenarios. The RT_{ER} is displayed for time to 99%, 75%, and 50% of steady state concentration (t_{99}, t_{75}, and t_{50}) at downstream boundary of reach.

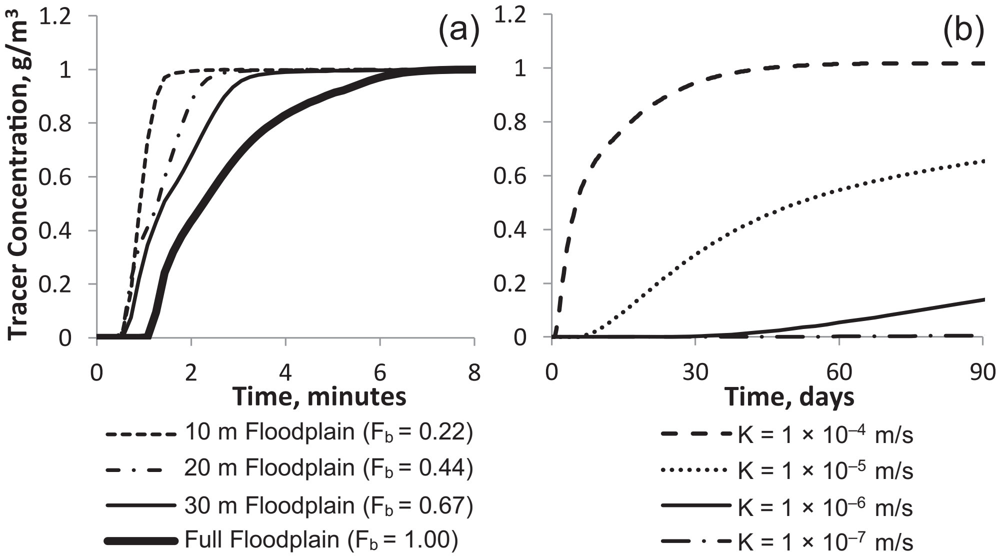

Figure 9. (a) Conservative tracer breakthrough curves for stormflow scenarios at the center of mass flux exiting the most upstream inset floodplain segment and (b) breakthrough curves at upwelling cell 1 m downstream of in-stream structure for summer base flow. To give a better estimate of the residence time on the inset floodplain, the breakthrough tracer curves were taken one cell away from the interface between the main channel and inset floodplain. See Figure 10 for why this particular model cell was chosen. $K = 1 \times 10^{-8}$ m/s is omitted because there is no measurable change in concentration over 90 days.

times, we corrected the inset floodplain t_{50} by subtracting the channel t_{50} for the adjacent channel for all inset floodplain segments. The residence times on individual inset floodplains increased with the floodplain length with a t_{50} of 0.79, 0.99, 1.02, and 1.35 minutes for F_b of 0.22, 0.44, 0.67, and 1.00, respectively.

Structure-induced hyporheic flow cells have a wide range of residence times. The majority (60%) of the mass flux reentering the channel from the structure-induced hyporheic flow cells did so within 1 m

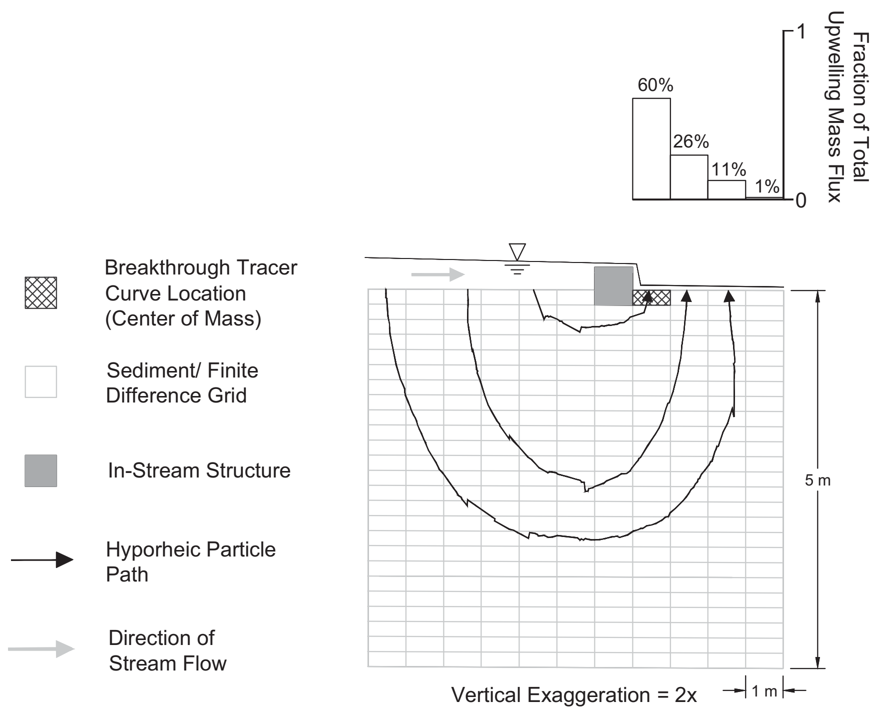

Figure 10. Location where breakthrough curves and residence times in the in-stream structure-induced hyporheic zone were output from the model. The fraction of total mass flux exiting the hyporheic zone is shown for cells 1, 2, 3, and 4 m from center of the in-stream structure at steady state for summer base flow scenarios. Hyporheic flow paths are from particle tracking.

downstream of the in-stream structures for steady state solute concentrations (Figure 10). We therefore estimated the t_{50} in the hyporheic zone as the flux-weighted average t_{50} from the breakthrough tracer curves for cells upwelling into the stream within 1 m of the in-stream structures (three cells at the upstream structure and two cells at the downstream structure). The breakthrough tracer curves with a t_{50} closest to the flux-weighted average t_{50} of these five hyporheic cells (i.e., the model cells just downstream of each structure, Figure 10) are plotted for visualization in Figure 9b. It took longer to reach the steady state solute concentration for lower K. For example, steady state was reached at 40 days for K = 1×10^{-4} m/s, yet less than 1% of the steady state concentration was reached after 90 days for K = 1×10^{-7} m/s. The t_{50} increased from approximately 6 to 300 days as K increased from 1×10^{-4} to 1×10^{-6} m/s.

3.4. Fraction of Year That Storage Occurs

In-stream structure-induced hyporheic flow only occurred when floodplain groundwater levels were relatively low, thus reducing groundwater gaining in the channel. For the most recent full year of groundwater data available (December 2009 to December 2010), this occurred for approximately 20% of the year, during dry periods in the summer and early fall. By comparison, the inset floodplains were only active when the stream stage was higher than the inset floodplain elevation (0.5 m above thalweg), or approximately 1% of the year for the most recent full year of stream stage data (May 2011 to May 2012). The surface retention due to in-stream structures increased the channel median residence time by at least 10% for flow depths up to 0.35 m. Surface retention due to in-stream structures was expected for 90% of the year, also based on data from May 2011 to May 2012. Surface retention due to in-stream structures was not expected during storm events, but periods where flow was high enough to prevent such retention generally occurred for less than 24 consecutive hours.

4. Discussion

4.1. Natural Controls on Hydraulics and Solute Retention

In-stream structure-induced hyporheic flow occurred for summer base flow scenarios but not winter base flow or stormflow scenarios (Figure 6). Such seasonal variation was also found in *Wondzell and Swanson* [1996] as the hyporheic flux through a gravel bar was 0.8% of streamflow for summer base flow, 0.02% for winter base flow, and less than 0.01% during stormflow. Our study estimated a lower fraction of streamflow entering the in-stream structure-induced hyporheic zone ($Q_{F\text{-}HZ}$) for summer base flow, winter base flow, and stormflow conditions than *Wondzell and Swanson* [1996]. This was because we studied a stream with a higher degree of gaining, and lower hydraulic conductivity (K). Our variation in hyporheic flow between summer and winter base flow scenarios was due more to variation in groundwater levels than variation in surface water levels. This agrees with other studies on first-order to third-order streams where ambient groundwater recharge was found to limit hyporheic flow [*Hester and Doyle*, 2008; *Sawyer and Cardenas*, 2012]. *Lautz and Siegel* [2006] found that hyporheic flow occurred for gaining and not losing conditions, while our study found that hyporheic flow occurred for slightly gaining and not highly gaining conditions. Both studies indicate that hyporheic flow generally requires the degree of gaining to be within a fairly narrow range.

In-stream structure-induced hyporheic flow was eliminated during stormflow scenarios when the stream stage was more than twice the height of the in-stream structure. This caused the head drop across the in-stream structure to approach the stream slope eliminating the hydraulic gradient that drives hyporheic flow. *Hester and Doyle* [2008] also came to this conclusion when performing a sensitivity analysis on structure size and stream depth, while *Crispell and Endreny* [2009] found that hyporheic flow did not occur at cross vanes during stormflows. We also found that there was greater hyporheic flow for the downstream weir (Figure 6) due to the greater head drop across the step.

For the range of stream sediment K used in this study, the hyporheic zone did not have a significant effect on overall stream reach residence times because the proportion of surface flow that cycled through the hyporheic zone was so small. By contrast, surface storage above inset floodplains dominated reach–level retention or transient storage in our model. Despite the fact that residence times on the inset floodplains were short (1–5 min), transient storage was still illustrated by a delay in reaching the steady state tracer concentration for the downstream channel breakthrough tracer curve when the tracer was added, and a delay in going back to a concentration of zero when the tracer was turned off (Figure 7). Surface storage for reach-level transient storage was similarly found for streams without restoration [*Jin and Ward*, 2005] as well as those with obstructions added [*Ensign and Doyle*, 2005; *Stofleth et al*., 2008]. Although not the focus of our study, surface storage also occurred in our model behind in-stream structures at base flow. Surface storage is illustrated by a decrease in channel flow velocity behind the in-stream structures and an increase in storage volume in the backwater areas upstream of structures, similar to field results found for baffles by *Ensign and Doyle* [2005]. The primary control on surface storage upstream of in-stream structures (during summer base flow) and on inset floodplains (during stormflow) is stream stage.

4.2. Stream Restoration Design Controls on Solute Retention

4.2.1. In-Stream Structure-Induced Hyporheic Retention

We found that in-stream structures only induced hyporheic flow when certain conditions were met. These conditions, outlined in section 4.1, included near-neutral groundwater environments, base flow stream stage, and K sufficiently large for a significant proportion of the streamflow to enter the hyporheic zone. Such conditions are necessary but not sufficient to insure water quality effects, as all reactants must also be present [*Schnoor*, 1996] and there must be sufficient residence time in the storage zone [*Zarnetske et al*., 2011, 2012]. For substantial improvements in stream water quality, all of these conditions would have to be met for a reasonable amount of the year.

Only 0.3% of channel flow traveled through the in-stream structure-induced hyporheic zone for a 90 m reach with two in-stream structures at our maximum K of 1×10^{-4} m/s. *Gordon et al*. [2013] similarly found that cross vanes in streams with primarily gravel and cobbles (with some sand and silt) resulted in 0.2%–0.4% streamflow entering the hyporheic zone for single structure over a $\sim$50 m reach. Their K is reasonably close to our maximum, so the slight differences in hyporheic flow are likely due to differences in the degree of gaining and structure height (our study at 0.3 m versus theirs at 0.44 and 0.75 m). Such hydrologic effects of in-stream structure-induced hyporheic flow are additive. Therefore, restoring a longer reach with the same structure spacing along the channel (i.e., structure density) can lead to a proportionally greater fraction of flow entering the hyporheic zone.

Equations (6) and (7) may be used to estimate the length of channel necessary to cycle a given proportion of stream water through the hyporheic zone. For example, cycling all stream water through the in-stream structure-induced hyporheic zone once ($Q_{F\text{-}HZ} = 1$) at Stroubles Creek would require approximately 3000 km of restored channel (for $K = 1 \times 10^{-6}$ m/s). This assumes 3000 km of third-order channel exist with dimensions and flow similar to Stroubles Creek. Restoring streams reaches this long is clearly not feasible. This indicates that in-stream structure-induced hyporheic exchange could not realistically cycle all the streamflow in this setting. The required length of stream would be substantially less with higher K (e.g., 30 km for $K = 1 \times 10^{-4}$ m/s) though this is still unrealistic. The groundwater conditions and K at Stroubles Creek are therefore not conducive to inducing significant in-stream structure-induced hyporheic flow.

From Darcy's Law, we expect that γ in equation (7) will be linearly related to the hydraulic gradient across the in-stream structures and the surface area of upwelling groundwater. The structure height is the primary control on the hydraulic gradient for neutral groundwater conditions. However, in highly gaining or losing situations, the hydraulic gradient from the groundwater to the stream is larger than that induced by the in-stream structure. This would effectively make the hydraulic gradient across the in-stream structure (and therefore γ) zero, in agreement with the hydraulic gradient dependence in *Hester and Doyle* [2008].

4.2.2. Inset Floodplain-Induced Surface Retention

Inset floodplain length and therefore fraction of bank with floodplains (F_b) control solute retention by inset floodplains. As these parameters increased, the fraction of streamflow that flows onto inset floodplains ($Q_{F\text{-}FP}$), the overall reach residence times enhancement ratio (RT_{ER}), the mass stored on inset floodplains, and the residence time on individual inset floodplain segments all increased (Figures 5, 8, and 9). However, all of these trends were nonlinear, and leveled off to varying degrees as floodplain length or F_b increased. For example, $Q_{F\text{-}FP}$ and RT_{ER} (for t_{50} and t_{75}) leveled off at F_b less than 1.0 (Figures 5 and 8) due to the relationship between momentum and topographic controls on flow onto inset floodplains. Channel flow generally has greater momentum (depth and velocity) at the outside of meander bends [*Leopold and Wolman*, 1960], resulting in flow for the full floodplain ($F_b = 1.0$) to be driven onto the floodplains primarily at the upstream end of meanders with this flow reentering the channel at the downstream end [*Naish and Sellin*, 1996]. The smaller inset floodplain segments ($F_b < 1$) added topographic controls to this phenomenon.

Table 4. Comparison of Retention Induced by In-Stream Structures and Inset Floodplains[a]

	Structure-Induced Hyporheic Zone	Inset Floodplain
Time when retention element dominant	Base flow	Stormflow
Approximate % of year when engaged	**20%**	1%
Fraction of flow that enters storage zone (Q_F)	0.00003–0.003	**0.3–0.6**
Steady state storage (M/M_{MC})	**2.8**	0.2–0.5
Median residence time in storage zone (t_{50})	**6–300 days**	0.8–1.4 min
Reach residence time enhancement ratio (RT_{ER})	1.0	**1.1–3.3**

[a]Bold text indicates the restoration practice that leads to more retention for each metric.

Water from the main channel was forced to reenter the channel wherever the inset floodplain segments ended, cycling channel water more effectively. This topographic control is what caused the $Q_{F\text{-}FP}$ and RT_{ER} to increase from $F_b = 0.00$ to $F_b = 0.67$. For $F_b = 0.67$, the flow is not limited by the topographic controls, resulting in similar $Q_{F\text{-}FP}$ and RT_{ER} to $F_b = 1.0$.

Equations (8) and (9) can be used to estimate the length of channel with inset floodplains required to increase the overall stream residence time by a certain amount during stormflow. For example, for $F_b = 0.67$ it would require approximately 200 m of restored channel at Stroubles Creek to increase the overall reach residence time by 20% ($RT_{ER} = 1.2$). Because this calculation involves extrapolation beyond our modeled reach, it should be viewed as an estimate. Furthermore, the specific coefficients in equations (8) and (9) were based on the stormflow hydraulics, inset floodplain geometry, and sinuosity of Stroubles Creek and may not be appropriate for other streams. Nevertheless, the basic form of the equations should be more widely applicable and is a useful heuristic to understand inset floodplain restoration effects on stream residence times.

The relationships between inset floodplain morphology, restored reach length, and retention are useful for understanding how restored streams function. Nevertheless, due to the low stream residence times over inset floodplains, the effect this restoration practice has on dissolved pollutants is expected to be minimal. We acknowledge that modifications of these inset floodplains, such as increasing their width or adding thicker vegetation, may increase residence times, but this is unlikely to substantially alter this basic conclusion.

4.3. Comparison of Inset Floodplains and In-Stream Structures

One of the key findings of this study is that inset floodplains and in-stream structure-induced hyporheic zones retained solutes in dramatically different ways (Table 4). For example, while inset floodplains retained solutes for stormflow scenarios, in-stream structures retained solutes for summer base flow scenarios. Due to these hydraulic differences, retention in the hyporheic zone occurred for a larger portion of the year than retention on floodplains. On the other hand, floodplains induced higher exchange flows than structure-induced hyporheic flow when such flows occurred. At least 10 km of stream with two structures every 90 m would be needed to cycle the same amount of water through the hyporheic zone as flows onto the inset floodplains of our 90 m model reach (depending on K and F_b).

The mass stored in the in-stream structure-induced hyporheic zone at steady state transport was up to an order of magnitude larger than that stored on inset floodplains at steady state. Nevertheless, mass storage in the hyporheic zone can be either greater or less than that on inset floodplains depending on season and K because steady state is reached within minutes for inset floodplains (Figure 9a) but takes days to months in the hyporheic zone (Figure 9b). Residence times in the hyporheic zone were several orders of magnitude larger than those on the inset floodplains (consistent with *Helton et al.* [2012]) and are therefore expected to lead to more complete reactions in many cases.

Surface storage due to inset floodplains occurred during approximately six storm events per year, or for ~1% of the year (Table 4). This frequency of inset floodplain engagement leaves seemingly little chance for a water quality effect. Yet even this level of engagement is substantially more than bankfull floodplains that are typically inundated once every 1–2 years [*Soar and Thorne*, 2011]. Furthermore, during stormflow events far more than 1% of annual streamflow (e.g., ~36% during the 10 days with the greatest flow [*USGS*, 2013]) and between 40% and 90% of annual pollutant loading occurs [*Owens et al.*, 1991; *Pionke et al.*, 1999; *Royer* *et al.*, 2006], making inset floodplains potentially more important than inundation frequencies suggest. Several studies suggest that restoration efforts should focus on retention during these high pollutant loading yet low probability events [*Bayley*, 1991; *Hein et al.*, 2003; *Rohde et al.*, 2006]. By contrast, in-stream structure-induced hyporheic retention occurred for approximately 20% of the year at Stroubles Creek (summer base flow) while surface storage behind structures reduced overall reach velocities for over 90% of the year. Depending on the groundwater conditions for a given stream, these percentages could vary considerably.

Given the magnitude of difference in exchange rates, residence times, and storage durations of the two restoration practices, we conclude that neither in-stream structure-induced hyporheic zones nor inset floodplain will generally have sufficient residence times and percent of flow *simultaneously* (Table 4) to impact water quality via biochemical reactions. This limits the ability of these restoration practices to cause reductions of many dissolved surface water contaminants moving downstream, at least in streams where *K* is within or lower than the range we used in our model. For example, the fraction of streamflow that entered the hyporheic zone for the 90 m reach modeled in this study is too low to have a significant impact on surface water quality. Yet the residence times were likely long enough for reactions of pollutants (e.g., excess nitrate) to occur in the induced hyporheic zones [*Zarnetske et al.*, 2011, 2012]. For example, for hyporheic flow through a gravel bar of a third-order stream *Zarnetske et al.* [2011] found that nitrification occurred for the first 7 h of hyporheic flow, at which point denitrification became the dominant process with the concentration approaching 0 after 30 h. As these residence times are orders of magnitude less than those predicted in our study, complete reactions would be expected. In contrast, a significant fraction of stream water flows onto inset floodplains (Figure 5). Yet the t_{50} on the inset floodplains are on the order of minutes, and are generally too low to expect complete pollutant reactions to occur [*Zarnetske et al.*, 2011, 2012]. Nevertheless, denitrification is observed by *Böhlke et al.* [2004] with storage residence times on the order of minutes during transient storage experiments, indicating that some denitrification may occur on inset floodplains. These rates are expected to be substantially less than those found where there are higher residence times [*Roley et al.*, 2012b, 2012a].

The benefits of stream restoration are numerous and include reducing erosion, protecting infrastructure, and various social benefits [*Kenney et al.*, 2012]. However, within the range of stream characteristics (e.g., K) evaluated in this study, we do not anticipate a significant reduction in surface water dissolved contaminants moving downstream as a result of inset floodplains or in-stream structure-induced hyporheic exchange.

4.4. Evaluation of Key Model Parameters and Assumptions

We performed a sensitivity analysis to estimate the impact of the selection of the Manning's roughness coefficient (n) and the transverse mixing coefficient for surface water (ε_t) used for this study. We varied n for the main channel and inset floodplain at endpoints of a reasonable range of values (0.025–0.05 for the main channel and 0.05–0.1 for the inset floodplain) [*McCuen*, 2005]. Stormflow models were run with all combinations of the minimum, maximum, and base n for the main channel and inset floodplain. The maximum changes in flow and residence time occurred when the minimum n was used for the channel and the maximum n was used for the inset floodplain or vice–a–versa, so only these two cases were analyzed for $F_b = 0.00$, 0.22, 0.44, 0.67, and 1.0. Between these two extremes, RT_{ER} varied by less than 15%, $Q_{F\text{-}FP}$ varied by no more than 50%, and t_{50} on an individual inset floodplain segment varied by no more than 40%. These maximum variations are each less than an order of magnitude, yet the difference in magnitude for residence times and flow between the inset floodplains and structure-induced hyporheic zone is several orders of magnitude (Table 4). Additionally, there was no change in the mass stored on the inset floodplains with n. As a result, our conclusions from Table 4 (i.e., section 4.3) would be unaltered by selecting alternative values for n.

ε_t was also varied across a range of reasonable values for natural channels (i.e., 0.01–0.2 m^2/s) [*Fischer*, 1973; *Fischer et al.*, 1979], with stormflow models run for $F_b = 0.00$, 0.22, 0.44, 0.67, and 1.0. RT_{ER} varied by a maximum of 35%, and the transport times on individual inset floodplain varied by no more than a factor of 2. There was generally greater variation in transport time with ε_t for the longer inset floodplain segments (higher F_b), due to increased mixing associated with a higher ε_t. There was no change in the mass stored on the inset floodplains or flow onto the inset floodplains with ε_t because ε_t is only used for solute transport calculations. The maximum variations are each less than an order of magnitude, yet the difference in residence times between floodplains and the structure-induced hyporheic zone was several orders of magnitude (Table 4), so the comparison between the two is again unaltered. In addition, both n and ε_t were held constant when evaluating the effect of variations in parameters such as F_b, K, and reach length (e.g., Figures 5–9), so conclusions drawn from the overall trends present in those figures are also independent of these parameters.

We modeled our stormflow scenario as steady state, yet stormflow conditions are transient by nature. This would affect our results for both inset floodplains and structure-induced hyporheic zones, yet should not affect our order-of-magnitude comparisons of the two storage zones. Fluctuations in surface water stage over short time periods can create short-term hyporheic zones in streambed sediment [*Zimmer and Lautz*, 2014] and stream banks [*Sawyer et al*., 2009]. The floodplain and bank K at Stroubles Creek is too low (1×10^{-8} m/s) for such rapid fluctuations to propagate far into the sediment matrix. Preferential flow in soil pipes and other macropores can increase exchange during storms [*Menichino et al*., 2014], but was beyond the scope of our study.

We assumed homogenous and isotropic sediment conditions for all groundwater modeling. We expect that bed heterogeneity and anisotropic conditions would increase the flux in the hyporheic zone and decrease residence times [*Salehin et al*., 2004; *Sawyer and Cardenas*, 2009] due to introduction of preferential flow paths. *Sawyer and Cardenas* [2009] concluded that assuming isotropic and homogeneous conditions was reasonable, while *Salehin et al*. [2004] found that changes in hyporheic flow varied by 20% or less. In these studies, the changes in flow and median residence time are by less than an order of magnitude, but added a great deal of additional spatial variability.

We assumed a constant channel slope for this model which omitted existing pools, riffles, and other natural stream features where a significant portion of naturally occurring hyporheic flow would occur [*Hester and Gooseff*, 2010; *Gordon et al*., 2013]. As a result, the hyporheic zones induced by the in-stream structures represented the entire hyporheic zone in the reach. This is consistent with our focus on the effect of restoration techniques, and thus we report hyporheic flux induced by in-stream structures rather than induced by natural features.

Our use of breakthrough tracer curves located at the center of mass flux leaving storage zones resulted in residence times that represented the overall system reasonably well, although the longest flow paths were omitted. Breakthrough tracer curves from cells at the downstream end of the inset floodplains, as well as from cells further than 1 m from the in-stream structures, indicated longer residence times than found at the center of mass flux. This study analyzes median residence times and not the entire residence time distribution. These results are sufficient for comparative purposes with the understanding that flow paths with residence times shorter and longer than the median residence time are also expected.

We did not perform a grid size sensitivity analysis because MIKE SHE required over a week to run a single model when the grid size was reduced by half (to 0.5 m by 0.5 m), which would make our sensitivity analysis prohibitive and change the overall nature of our study. Such a sensitivity analysis was performed in *Wondzell et al*. [2009] for a small mountain stream. Reducing the grid size from 1 m by 1 m to 0.5 m by 0.5 m led to $\sim$15% increase in hyporheic flow, and a grid size of 0.125 m by 0.125 m led to $\sim$30% increase in hyporheic flow from a 1 m by 1 m grid. In our study, the effects of such grid adjustments would not change the trends of hyporheic flux versus controlling parameters, nor the relative comparisons with inset floodplain flux given the multiple orders of magnitude difference we observed.

5. Conclusions

Retention of channel water in off-channel storage zones such as the hyporheic zone or inset floodplains is typically required for significant contaminant reactions to occur in stream systems. We used coupled surface water-groundwater modeling of hydraulics and solute transport (MIKE SHE) to analyze the effects of in-stream structures and inset floodplains on solute retention in streams, while varying hydraulic and geologic conditions, and design parameters. In-stream structures-induced solute retention in the hyporheic zone at locations where there were relatively neutral groundwater conditions during base flow. Such hyporheic flow was highly dependent on K. Inset floodplain-induced surface retention occurred only during stormflow when the stream stage was higher than the inset floodplain elevation.

Simple scaling relationships generated from our model output are useful for understanding the effects of design parameters or constraints on hydraulic retention (equations (6–9)). For example, increasing the fraction of the stream bank with inset floodplains increased exchange flow and reach residence times up to a point, after which it leveled off. Increasing the length of restored reach increased hydraulic retention in both structure-induced hyporheic zones and inset floodplains.

Inset floodplains and in-stream structure-induced hyporheic zones retained solutes in dramatically different ways (Table 4). For example, in-stream structure-induced hyporheic retention occurred for approximately 20% of the year (primarily during summer), while inset floodplains led to surface storage for approximately 1% of the year (during storms). The fraction of streamflow passing onto inset floodplains was one to three orders of magnitude higher than that cycling through the in-stream structure-induced hyporheic zone, while hyporheic zone residence times were approximately three to five orders of magnitude larger than for inset floodplains. Further, the solute mass stored in the hyporheic zone at steady state was approximately one order of magnitude larger than that stored over the inset floodplains.

Given these distinctions, within the range of stream characteristics explored in this study (e.g., K), neither structure-induced hyporheic zones nor inset floodplains were expected to simultaneously have both sufficient residence time and sufficient percent of flow to allow substantial reaction of dissolved surface water contaminants. The corresponding effect on dissolved pollutants from these stream restoration practices would therefore likely be minimal.

Acknowledgments
The authors thank the Charles E. Via Jr. Endowment at Virginia Tech and a NSF grant to E. T. Hester and D. Scott (ENG-CBET-1066817) for providing financial support to David Azinheira. Views expressed in this paper are those of the authors and not necessarily those of the NSF. We thank the Danish Hydraulic Institute for providing MIKE-SHE at a reduced rate. We also thank the Virginia Tech Institute for Critical Technology and Applied Sciences (ICTAS) Sustainable Water program for funds for maintenance and monitoring activities at the StREAM Lab. We thank Steven Wondzell, F. Douglas Shields Jr., and four anonymous reviewers for helpful comments on this manuscript. Data described in this paper are available upon request by emailing the corresponding author.

References

Alexander, R. B., R. A. Smith, and G. E. Schwarz (2000), Effect of stream channel size on the delivery of nitrogen to the Gulf of Mexico, *Nature*, *403*(6771), 758–761, doi:10.1038/35001562.

Anderson, M. P., and W. W. Woessner (1992), *Applied Groundwater Modeling: Simulation of Flow and Advective Transport*, Academic, San Diego, Calif.

Anderson, J. K., S. M. Wondzell, M. N. Gooseff, and R. Haggerty (2005), Patterns in stream longitudinal profiles and implications for hyporheic exchange flow at the H.J. Andrews Experimental Forest, Oregon, USA, *Hydrol. Processes*, *19*(15), 2931–2949, doi:10.1002/hyp.5791.

Arcement, G. J., and V. R. Schneider (1989), *Guide for Selecting Manning's Roughness Coefficients for Natural Channels and Flood Plains*, vol. 38, U.S. Gov. Print. Off., Washington, D. C.

Bayley, P. B. (1991), The flood pulse advantage and the restoration of river-floodplain systems, *Regul. Rivers*, *6*(2), 75–86, doi:10.1002/RRR.3450060203.

BenDor, T., J. Sholtes, and M. W. Doyle (2009), Landscape characteristics of a stream and wetland mitigation banking program, *Ecol. Appl.*, *19*(8), 2078–2092, doi:10.1890/08–1803.1.

Berg, J., J. Burch, D. Cappuccitti, S. Filoso, L. Fraley-McNeal, D. Goerman, N. Hardman, S. Kaushal, D. Medina, and M. Meyers (2014), *Recommendations of the Expert Panel to Define Removal Rates for Individual Stream Restoration Projects*, Chesapeake Bay Program.

Bernhardt, E. S., et al. (2005), Synthesizing U.S. river restoration efforts, *Science*, *308*(5722), 636–637, doi:10.1126/science.1109769.

Boano, F., C. Camporeale, R. Revelli, and L. Ridolfi (2006), Sinuosity-driven hyporheic exchange in meandering rivers, *Geophys. Res. Lett.*, *33*, L18406, doi:10.1029/2006GL027630.

Böhlke, J. K., J. W. Harvey, and M. A. Voytek (2004), Reach-scale isotope tracer experiment to quantify denitrification and related processes in a nitrate-rich stream, midcontinent United States, *Limnol. Oceanogr. Methods*, *49*(3), 821–838.

Box, J. (1996), Setting objectives and defining outputs for ecological restoration and habitat creation, *Restor. Ecol.*, *4*(4), 427–432, doi:10.1111/J.1526-100X.1996.TB00196.X.

Brunke, M., and T. Gonser (1997), The ecological significance of exchange processes between rivers and groundwater, *Freshwater Biol.*, *37*(1), 1–33, doi:10.1046/J.1365–2427.1997.00143.X.

Buchanan, B., M. Walter, G. Nagle, and R. Schneider (2012), Monitoring and assessment of a river restoration project in central New York, *River Res. Appl.*, *28*(2), 216–233, doi:10.1002/rra.1453.

Bukaveckas, P. A. (2007), Effects of channel restoration on water velocity, transient storage, and nutrient uptake in a channelized stream, *Environ. Sci. Technol.*, *41*(5), 1570–1576, doi:10.1021/ES061618X.

Calver, A. (2005), Riverbed permeabilities: Information from pooled data, *Ground Water*, *39*(4), 546–553, doi:10.1111/J.1745–6584.2001.TB02343.X.

Cardenas, M. B., and J. L. Wilson (2006), The influence of ambient groundwater discharge on exchange zones induced by current-bedform interactions, *J. Hydrol.*, *331*(1), 103–109, doi:10.1016/J.JHYDROL.2006.05.012.

Cardenas, M. B., J. L. Wilson, and V. A. Zlotnik (2004), Impact of heterogeneity, bed forms, and stream curvature on subchannel hyporheic exchange, *Water Resour. Res.*, *40*, W08307, doi:10.1029/2004WR003008.

Changxing, S., G. Petts, and A. Gurnell (1999), Bench development along the regulated, lower River Dee, UK, *Earth Surf. Processes Landforms*, *24*(2), 135–149.

Chin, A. (2003), The geomorphic significance of step–pools in mountain streams, *Geomorphology*, *55*(1–4), 125–137, doi:10.1016/S0169–555X(03)00136-3.

Chin, A., S. Anderson, A. Collison, B. J. Ellis-Sugai, J. P. Haltiner, J. B. Hogervorst, G. M. Kondolf, L. S. O'Hirok, A. H. Purcell, and A. L. Riley (2009), Linking theory and practice for restoration of step-pool streams, *Environ. Manage.*, *43*(4), 645–661, doi:10.1007/S00267-008-9171-X.

Cirpka, O. A., and P. K. Kitanidis (2000), An advective-dispersive stream tube approach for the transfer of conservative-tracer data to reactive transport, *Water Resour. Res.*, *36*(5), 1209–1220, doi:10.1029/1999WR900355.

Cirpka, O. A., E. O. Frind, and R. Helmig (1999), Numerical simulation of biodegradation controlled by transverse mixing, *J. Contam. Hydrol.*, *40*(2), 159–182, doi:10.1890/070080.

Copeland, C. (2006), Water quality: Implementing the Clean Water Act, *Congr. Res. Serv. Rep. 36*, Congressional Research Service, Washington, D. C.

Craig, L. S., et al. (2008), Stream restoration strategies for reducing river nitrogen loads, *Frontiers Ecol. Environ.*, *6*(10), 529–538, doi:10.1890/070080.

Creswell, J. E., S. C. Kerr, M. H. Meyer, C. L. Babiarz, M. M. Shafer, D. E. Armstrong, and E. E. Roden (2008), Factors controlling temporal and spatial distribution of total mercury and methylmercury in hyporheic sediments of the Allequash Creek wetland, northern Wisconsin, *J. Geophys. Res.*, *113*, G00C02, doi:10.1029/2008JG000742.

Crispell, J. K., and T. A. Endreny (2009), Hyporheic exchange flow around constructed in-channel structures and implications for restoration design, *Hydrol. Processes*, *23*(8), 1158–1168, doi:10.1002/hyp.7230.

Daniluk, T. L., L. K. Lautz, R. P. Gordon, and T. A. Endreny (2012), Surface water-groundwater interaction at restored streams and associated reference reaches, *Hydrol. Processes*, *27*(25), 3730–3746, doi:10.1002/hyp.9501.

DHI (Danish Hydraulic Institute) (2011), *MIKE SHE User Manual*, vol. 2, *Reference Guide*, DHI, Hørsholm, Denmark.

Endreny, T., L. Lautz, and D. Siegel (2011a), Hyporheic flow path response to hydraulic jumps at river steps: Flume and hydrodynamic models, *Water Resour. Res.*, *47*, W02517, doi:10.1029/2009WR008631.

Endreny, T., L. Lautz, and D. Siegel (2011b), Hyporheic flow path response to hydraulic jumps at river steps: Hydrostatic model simulations, *Water Resour. Res.*, *47*, W02518, doi:10.1029/2010WR010014.

Ensign, S. H., and M. W. Doyle (2005), In-channel transient storage and associated nutrient retention: Evidence from experimental manipulations, *Limnol. Oceanogr. Methods*, *50*(6), 1740–1751.

Filoso, S., and M. A. Palmer (2011), Assessing stream restoration effectiveness at reducing nitrogen export to downstream waters, *Ecol. Appl.*, *21*(6), 1989–2006, doi:10.1890/10–0854.1.

Fischer, H. B. (1973), Longitudinal dispersion and turbulent mixing in open-channel flow, *Annu. Rev. Fluid Mech.*, *5*(1), 59–78, doi:10.1146/annurev.fl.05.010173.000423.

Fischer, H. B., J. E. List, R. C. Y. Koh, J. Imberger, and N. H. Brooks (1979), *Mixing in Inland and Coastal Waters*, vol. xiv, 483 pp., Academic, N. Y.

FISRWG (Federal Interagency Stream Restoration Working Group) (1998), Stream corridor restoration: Principles, processes, and practices, Rep. 0934213593 9780934213592, Fed. Interagency Stream Restoration Working Group, Washington, D. C.

Freeze, R. A., and J. A. Cherry (1979), *Groundwater*, Prentice Hall, Englewood Cliffs, N. J.

Gelhar, L. W., C. Welty, and K. R. Rehfeldt (1992), A critical review of data on field-scale dispersion in aquifers, *Water Resour. Res.*, *28*(7), 1955–1974, doi:10.1029/92WR00607.

Giammarco, P., E. Todini, and P. Lamberti (1996), A conservative finite elements approach to overland flow: The control volume finite element formulation, *J. Hydrol.*, *175*(1), 267–291, doi:10.1016/S0022–1694(96)80014-X.

Gordon, R. P., L. K. Lautz, and T. L. Daniluk (2013), Spatial patterns of hyporheic exchange and biogeochemical cycling around cross-vane restoration structures: Implications for stream restoration design, *Water Resour. Res.*, *49*, 2040–2055, doi:10.1002/WRCR.20185.

Graham, D. N., and M. B. Butts (2005), Flexible, integrated watershed modelling with MIKE SHE, in *Watershed Models*, edited by V. P. Singh, and D. K. Frevert, pp. 245–272, CRC Press, Boca Raton, Fla.

Haycock, N. E., and T. P. Burt (1993), Role of floodplain sediments in reducing the nitrate concentration of subsurface run-off: A case study in the Cotswolds, UK, *Hydrol. Processes*, *7*(3), 287–295, doi:10.1002/hyp.3360070306.

Heeren, D. M., G. A. Fox, R. B. Miller, D. E. Storm, A. K. Fox, C. J. Penn, T. Halihan, and A. R. Mittelstet (2011), Stage-dependent transient storage of phosphorus in alluvial floodplains, *Hydrol. Processes*, *25*(20), 3230–3243, doi:10.1002/hyp.8054.

Hein, T., C. Baranyi, G. J. Herndl, W. Wanek, and F. Schiemer (2003), Allochthonous and autochthonous particulate organic matter in floodplains of the River Danube: The importance of hydrological connectivity, *Freshwater Biol.*, *48*(2), 220–232, doi:10.1046/j.1365–2427.2003.00981.x.

Helton, A. M., G. C. Poole, R. A. Payn, C. Izurieta, and J. A. Stanford (2012), Relative influences of the river channel, floodplain surface, and alluvial aquifer on simulated hydrologic residence time in a montane river floodplain, *Geomorphology*, *205*(15), 17–26, doi:10.1016/j.geomorph.2012.01.004.

Henderson, F. M. (1966), *Open Channel Flow*, vol. xxii, 522 pp., Macmillan, N. Y.

Hester, E. T., and M. W. Doyle (2008), In-stream geomorphic structures as drivers of hyporheic exchange, *Water Resour. Res.*, *44*, W03417, doi:10.1029/2006WR005810.

Hester, E. T., and M. N. Gooseff (2010), Moving beyond the banks: Hyporheic restoration is fundamental to restoring ecological services and functions of streams, *Environ. Sci. Technol.*, *44*(5), 1521–1525, doi:10.1021/es902988n.

Hines, S. L., and A. E. Hershey (2011), Do channel restoration structures promote ammonium uptake and improve macroinvertebrate-based water quality classification in urban streams?, *Inland Waters*, *1*(2), 133–145.

Holtz, R. D., and W. D. Kovacs (1981), *An Introduction to Geotechnical Engineering*, Prentice Hall, Englewood Cliffs, N. J.

Horritt, M., and P. Bates (2001), Predicting floodplain inundation: Raster-based modelling versus the finite element approach, *Hydrol. Processes*, *15*(5), 825–842, doi:10.1002/hyp.188.

Hromadka, T., C. Berenbrock, J. Freckleton, and G. Guymon (1985), A two-dimensional dam-break flood plain model, *Adv. Water Resour.*, *8*(1), 7–14, doi:10.1016/0309–1708(85)90074-0.

Jin, H.-S., and G. M. Ward (2005), Hydraulic characteristics of a small Coastal Plain stream of the southeastern United States: Effects of hydrology and season, *Hydrol. Processes*, *19*(20), 4147–4160, doi:10.1002/hyp.5878.

Keaton, J. N., T. Messinger, and E. J. Doheny (2005), *Development and Analysis of Regional Curves for Streams in the Non-Urban Valley and Ridge Physiographic Province, Maryland, Virginia, and West Virginia*, U.S. Dep. of the Interior, U.S. Geol. Surv, Denver, Colo.

Kenney, M. A., P. R. Wilcock, B. F. Hobbs, N. E. Flores, and D. C. Martínez (2012), Is urban stream restoration worth it?, *J. Am. Water Resour. Assoc.*, *48*(3), 603–615, doi:10.1111/J.1752-1688.2011.00635.X.

Kim, H., H. F. Hemond, L. R. Krumholz, and B. A. Cohen (1995), In-situ biodegradation of toluene in a contaminated stream, *Environ. Sci. Technol.*, *29*(1), 108–116, doi:10.1021/es00001a014.

Kondolf, G. M., and E. R. Micheli (1995), Evaluating stream restoration projects, *Environ. Manage.*, *19*(1), 1–15, doi:10.1007/BF02471999.

Lautz, L. K., and D. L. Siegel (2006), Modeling surface and ground water mixing in the hyporheic zone using MODFLOW and MT3D, *Adv. Water Resour.*, *29*(11), 1618–1633, doi:10.1016/j.advwatres.2005.12.003.

Leopold, L. B., and M. G. Wolman (1960), River meanders, *Geol. Soc. Am. Bull.*, *71*(6), 769–793.

Mason, S. J. K., B. L. McGlynn, and G. C. Poole (2012), Hydrologic response to channel reconfiguration on Silver Bow Creek, Montana, *J. Hydrol. [Amsterdam]*, *438*(1), 125–136, doi:10.1016/j.jhydrol.2012.03.010.

McCuen, R. (2005), *Hydrologic Analysis and Design*, Prentice Hall, Englewood Cliffs, N. J.

Menichino, G. T., A. S. Ward, and E. T. Hester (2014), Macropores as preferential flow paths in meander bends, *Hydrol. Processes*, *28*(3), 482–495, doi:10.1002/hyp.9573.

Moussa, R., and C. Bocquillon (2000), Approximation zones of the Saint-Venant equations f flood routing with overbank flow, *Hydrol. Earth Syst. Sci. Discuss.*, *4*(2), 251–260, doi:10.5194/hess-4–251-2000.

Nagaoka, H., and S. Ohgaki (1990), Mass transfer mechanism in a porous riverbed, *Water Res.*, *24*(4), 417–425, doi:10.1016/0043–1354(90)90223-S.

Naish, C., and R. Sellin (1996), Flow structure in a large-scale model of a doubly meandering compound river channel, in Coherent Flow Structures in Open Channels, pp. 631–654, John Wiley & Sons, N. Y.

Noe, G. B., and C. R. Hupp (2007), Seasonal variation in nutrient retention during inundation of a short-hydroperiod floodplain, *River Res. Appl.*, *23*(10), 1088–1101, doi:10.1002/rra.1035.

Noe, G. B., and C. R. Hupp (2009), Retention of riverine sediment and nutrient loads by Coastal Plain floodplains, *Ecosystems*, *12*(5), 728–746, doi:10.1007/S10021-009-9253-5.

Opperman, J. J., G. E. Galloway, J. Fargione, J. F. Mount, B. D. Richter, and S. Secchi (2009), Sustainable floodplains through large-scale reconnection to rivers, *Science*, *326*(5959), 1487–1488, doi:10.1126/science.1178256.

Owens, L. B., W. M. Edwards, and R. W. Keuren (1991), Baseflow and stormflow transport of nutrients from mixed agricultural watersheds, *J. Environ. Qual.*, *20*(2), 407–414, doi:10.2134/jeq1991.00472425002000020012x.

Pionke, H. B., W. J. Gburek, R. R. Schnabel, A. N. Sharpley, and G. F. Elwinger (1999), Seasonal flow, nutrient concentrations and loading patterns in stream flow draining an agricultural hill-land watershed, *J. Hydrol.*, *220*(1–2), 62–73, doi:10.1016/S0022-1694(99)00064-5.

Radspinner, R., P. Diplas, A. F. Lightbody, and F. Sotiropoulos (2010), River training and ecological enhancement potential using in-stream structures, *J. Hydraul. Eng.*, *136*(12), 967–980, doi:10.1061/(ASCE)HY.1943-7900.0000260.

Rohde, S., M. Hostmann, A. Peter, and K. C. Ewald (2006), Room for rivers: An integrative search strategy for floodplain restoration, *Landscape Urban Plann.*, *78*(1–2), 50–70, doi:10.1016/j.landurbplan.2005.05.006.

Roley, S. S., J. L. Tank, and M. A. Williams (2012a), Hydrologic connectivity increases denitrification in the hyporheic zone and restored floodplains of an agricultural stream, *J. Geophys. Res.*, *117*, G00N04, doi:10.1029/2012JG001950.

Roley, S. S., J. L. Tank, M. L. Stephen, L. T. Johnson, J. J. Beaulieu, and J. D. Witter (2012b), Floodplain restoration enhances denitrification and reach-scale nitrogen removal in an agricultural stream, *Ecol. Appl.*, *22*(1), 281–297, doi:10.1890/11–0381.1.

Roni, P., T. J. Beechie, R. E. Bilby, F. E. Leonetti, M. M. Pollock, and G. R. Pess (2002), A review of stream restoration techniques and a hierarchical strategy for prioritizing restoration in pacific northwest watersheds, *N. Am. J. Fish. Manage.*, *22*(1), 1–20, doi: 10.1577/1548–8675(2002)022<0001:arosrt>2.0.co;2.

Rosgen, D. L. (2001), The cross-vane, W-Weir and J-Hook vane structures. . . Their description, design and application for stream stabilization and river restoration, in *Wetlands Engineering & River Restoration 2001*, pp. 1–22, American Society of Civil Engineers, Reno, Nevada, doi:10.1061/40581(2001)72.

Royall, D., L. Davis, and D. R. Kimbrow (2010), In-channel benches in small watersheds: Examples from the southern piedmont, *Southeast. Geogr.*, *50*(4), 445–467, doi:10.1353/sgo.2010.0012.

Royer, T. V., M. B. David, and L. E. Gentry (2006), Timing of riverine export of nitrate and phosphorus from agricultural watersheds in illinois: Implications for reducing nutrient loading to the Mississippi River, *Environ. Sci. Technol.*, *40*(13), 4126–4131, doi:10.1021/es052573n.

Salehin, M., A. I. Packman, and M. Paradis (2004), Hyporheic exchange with heterogeneous streambeds: Laboratory experiments and modeling, *Water Resour. Res.*, *40*, W11504, doi:10.1029/2003WR002567.

Sawyer, A. H., and M. B. Cardenas (2009), Hyporheic flow and residence time distributions in heterogeneous cross-bedded sediment, *Water Resour. Res.*, *45*, W08406, doi:10.1029/2008WR007632.

Sawyer, A. H., and M. B. Cardenas (2012), Effect of experimental wood addition on hyporheic exchange and thermal dynamics in a losing meadow stream, *Water Resour. Res.*, *48*, W10537, doi:10.1029/2011WR011776.

Sawyer, A. H., M. B. Cardenas, A. Bomar, and M. Mackey (2009), Impact of dam operations on hyporheic exchange in the riparian zone of a regulated river, *Hydrol. Processes*, *23*(15), 2129–2137, doi:10.1002/hyp.7324.

Sawyer, A. H., M. B. Cardenas, and J. Buttles (2011), Hyporheic exchange due to channel-spanning logs, *Water Resour. Res.*, *47*, W08502, doi: 10.1029/2011WR010484.

Schnoor, J. L. (1996), *Environmental Modeling: Fate and Transport of Pollutants in Water, Air, and Soil*, John Wiley, N. Y.

Soar, P. J., and C. R. Thorne (2011), Design discharge for river restoration, in *Stream Restoration in Dynamic Fluvial Systems, Geophys. Monogr. Ser.*, vol. 194, edited by A. Simon, S. J. Bennett and J. M. Castro, pp. 123–149, doi:10.1029/2010GM001009.

Stofleth, J. M., F. D. Shields Jr., and G. A. Fox (2008), Hyporheic and total transient storage in small, sand-bed streams, *Hydrol. Processes*, *22*(12), 1885–1894, doi:10.1002/hyp.6773.

Storey, R. G., K. W. F. Howard, and D. D. Williams (2003), Factors controlling riffle-scale hyporheic exchange flows and their seasonal changes in a gaining stream: A three-dimensional groundwater flow model, *Water Resour. Res.*, *39*, W01034, doi:10.1029/2002WR001367.

Thompson, W., C. W. Hession, and D. T. Scott (2012), StREAM Lab at Virginia Tech, *Resources Mag.*, *19*(2), 8–9.

Thoms, M. C., and J. M. Olley (2004), *The Stratigraphy, Mode of Deposition and Age of Inset Flood Plains on the Barwon-Darling River*, Australia, IAHS Publ, Moscow, Russia.

Tsai, C. W. (2005), Flood routing in mild-sloped rivers—Wave characteristics and downstream backwater effect, *J. Hydrol.*, *308*(1), 151–167, doi:10.1016/j.jhydrol.2004.10.027.

USGS (2013), How much water flows during a storm?, edited by USGS, U.S. Geol. Surv. [Available at http://ga.water.usgs.gov/edu/stormflow.html.]

Ward, A. S., M. Fitzgerald, M. N. Gooseff, T. J. Voltz, A. M. Binley, and K. Singha (2012), Hydrologic and geomorphic controls on hyporheic exchange during base flow recession in a headwater mountain stream, *Water Resour. Res.*, *48*, W04513, doi:10.1029/2011WR011461.

Weill, S., E. Mouche, and J. Patin (2009), A generalized Richards equation for surface/subsurface flow modelling, *J. Hydrol.*, *366*(1), 9–20, doi:10.1016/j.jhydrol.2008.12.007.

Wondzell, S. M. (2011), The role of the hyporheic zone across stream networks, *Hydrol. Processes*, *25*(22), 3525–3532, doi:10.1002/hyp.8119.

Wondzell, S. M., and F. J. Swanson (1996), Seasonal and storm dynamics of the hyporheic zone of a 4th-order mountain stream. I: Hydrologic processes, *J. N. Am. Benthol. Soc.*, *15*(1), 3–19.

Wondzell, S. M., J. LaNier, and R. Haggerty (2009), Evaluation of alternative groundwater flow models for simulating hyporheic exchange in a small mountain stream, *J. Hydrol.*, *364*(1), 142–151, doi:10.1016/j.jhydrol.2008.10.011.

Wood, P. J., and P. D. Armitage (1997), Biological effects of fine sediment in the lotic environment, *Environ. Manage.*, *21*(2), 203–217, doi:10.1007/s002679900019.

Wynn, T., C. Hession, and G. Yagow (2010), Stroubles Creek stream restoration, report 2007-WQIA-42, Virginia Dep. of Conserv. and Recreation and Virginia Tech Biol. Syst. Eng. Dep, Richmond, Va.

Zarnetske, J. P., R. Haggerty, S. M. Wondzell, and M. A. Baker (2011), Dynamics of nitrate production and removal as a function of residence time in the hyporheic zone, *J. Geophys. Res.*, *116*, G01025, doi:10.1029/2010JG001356.

Zarnetske, J. P., R. Haggerty, S. M. Wondzell, V. A. Bokil, and R. González-Pinzón (2012), Coupled transport and reaction kinetics control the nitrate source-sink function of hyporheic zones, *Water Resour. Res.*, *48*, W11508, doi:10.1029/2012WR011894.

Zimmer, M. A., and L. K. Lautz (2014), Temporal and spatial response of hyporheic zone geochemistry to a storm event, *Hydrol. Processes*, *28*(4), 2324–2337, doi:10.1002/hyp.9778.